Quantitative determination of mass-resolved ion densities in H_2-Ar inductively coupled radio frequency plasmas

M. Sode,[1, a)] T. Schwarz-Selinger,[1] and W. Jacob[1]

Max-Planck-Institut für Plasmaphysik, EURATOM Association, Boltzmannstraße 2, D-85748 Garching, Germany.

(Dated: 22 April 2013)

Inductively coupled H_2-Ar plasmas are characterized by an energy-dispersive mass spectrometer (plasma monitor), a retarding field analyzer, optical emission spectroscopy and a Langmuir probe. A procedure is presented that allows determining quantitatively the absolute ion densities of Ar^+, H^+, H_2^+, H_3^+ and ArH^+ from the plasma monitor raw signals. The calibration procedure considers the energy and mass-dependent transmission of the plasma monitor. It is shown that an additional diagnostic like a Langmuir probe or a retarding field analyzer is necessary to derive absolute fluxes with the plasma monitor. The conversion from fluxes into densities is based on a sheath and density profile model.

Measurements were conducted for a total gas pressure of 1.0 Pa. For pure H_2 plasmas the dominant ion is H_3^+. For mixed H_2-Ar plasmas the ArH^+ molecular ion is the most dominant ion species in a wide parameter range. The electron density n_e is around 3×10^{16} m^{-3} and the electron temperature T_e decreases from 5 to 3 eV with increasing Ar content. The dissociation degree was measured by actinometry. It is around 1.7 % nearly independent on Ar content. The gas temperature, estimated by the rotational distribution of the Q-branch lines of the H_2 Fulcher-α diagonal band ($v' = v'' = 2$) is estimated to (540±50) K.

PACS numbers: 52.20.-j, 52.25.-b, 52.70.-Nc, 52.80.Pj

Keywords: argon, hydrogen, ICP, ion densities, energy-resolved mass spectrometry, OES, Langmuir probe

[a)]Electronic mail: maik.sode@ipp.mpg.de

I. INTRODUCTION

H_2-containing plasmas have a wide range of technical applications in etching[1], film deposition[2–7] and surface passivation, hydrogenation and oxide reduction[8–11]. H_2-Ar mixtures were successfully applied for hydrogenation of thin film transistors[12] and to control the surface properties of polymers[13]. Hopf et al. observed chemical sputtering of hydrocarbon films with very high rates when energetic Ar and atomic hydrogen were interacting simultaneously[14]. Voitsenya et al. therefore proposed H_2-Ar discharges for the removal of hydrocarbon deposits in magnetic fusion devices[15]. However, to judge the effectiveness of such a method the absolute particle fluxes need to be known.

Qualitative mass-resolved measurements of different ion species in inductively coupled plasmas (ICP) of Ar and H_2 using an energy-dispersive mass spectrometer were carried out by Gudmundsson[16,17] and by Jang and Lee[18]. Gudmundsson showed ion energy distributions and uncorrected flux ratios of the H^+, H_2^+, H_3^+ and Ar^+ signals. Surprisingly the ArH^+ ion was not measured by Gudmundsson which was found to be the dominant ion for Ar containing H_2 discharges in our measurements. Jang and Lee measured ion species for the same system, but neglected H_3^+ which is the dominant ion species in a pure H_2 discharge. In general, with energy-dispersive mass spectrometers—often also named plasma monitors—signal intensities depending on the incoming ion fluxes are measured. In this work we are mainly aiming for ion densities because these can finally be compared with results of rate equation models. The relation between ion fluxes and the corresponding densities is established by plasma sheath models[19]. Kimura and Kasugai measured the electron temperature and electron density as well as the density of atomic hydrogen in H_2-Ar ICP plasmas and compared the results with a global model of the discharge[20]. They also presented modeling results for the mass-resolved ion densities but unfortunately they did not measure them.

Despite the numerous studies on hydrogen as well as H_2-Ar inductively coupled plasmas[16–18,20,21] no quantitative data on experimentally determined mass-resolved ion densities are available. Because this is also true for plasma characterization studies in general we want to outline in this article a procedure to derive absolute, mass-resolved ion densities from measurements with an energy-dispersive mass spectrometer. We present a comprehensive experimental study of H_2-Ar ICP plasmas. Quantitative results for the ion species present in the plasma are determined as a function of the Ar fraction. In addition, we measured electron tempera-

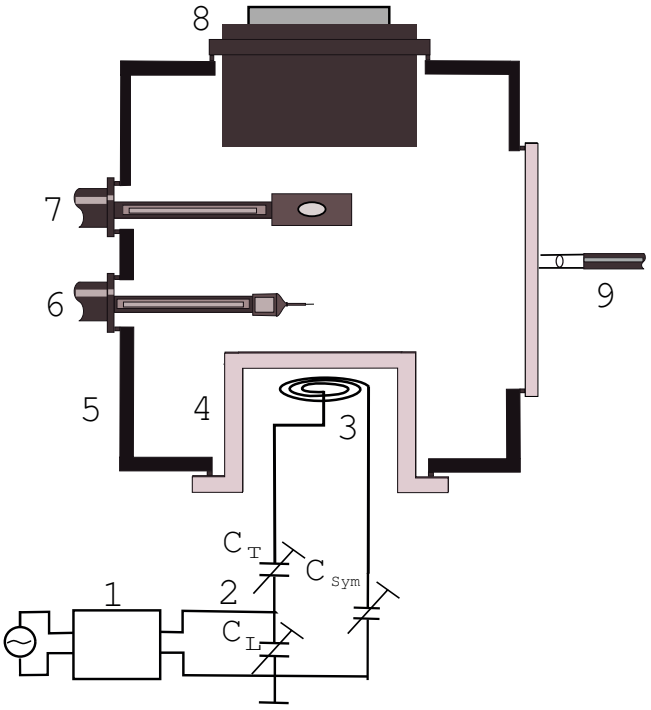

FIG. 1. Sketch of the experimental setup: 1 - RF generator, 2 - Π-type matching network, 3 - planar inductive coil, 4 - quartz dome, 5 - grounded vacuum chamber, 6 - Langmuir probe, 7 - retarding field analyzer, 8 - plasma monitor, 9 - light collecting system for the optical spectrometer.

ture and density, atomic hydrogen density, and gas temperature. This comprehensive set of experimentally determined plasma parameters provides a solid basis of input data for rate equation modeling[20,21]. Our final aim is to compare these data to results from such a rate equation model, but that will be topic of a forthcoming publication.

The article is organized as follows: A short description of the experimental setup is followed by a description of the evaluation process of the raw data measured with an energy-dispersive mass spectrometer, a retarding field analyzer, a Langmuir probe and by optical emission spectroscopy (OES). In Sect. IV the measured and evaluated results are discussed. The conclusions are presented in Sect. V.

II. EXPERIMENT

The experiments were conducted in an inductively coupled plasma reactor sketched in Fig. 1. The dimensions of the cylindrical stainless steel plasma chamber are similar to the geometry of the Gaseous Electronics Conference (GEC) reference cell[22] with a chamber

diameter of 250 mm and a total height of 360 mm. Compared to the initial design the distance between the two electrodes is larger, namely $l = 60$ mm. The discharge is generated by a planar coil with 5 turns and 100 mm in diameter that immerses 180 mm deep into the chamber. The coil is driven by a radio frequency (rf) generator with a maximum power of 600 Watt operating at 13.56 MHz (Dressler Cesar 136). In contrast to the initial GEC design, the coil is separated from the vacuum by a quartz dome[23]. Compared to a metallic shield this reduces power losses caused by eddy currents. The top part of the dome is 10 mm thick and acts as the dielectric window for the coil. The diameter of the quartz dome and the upper electrode is 131 mm. For matching of the rf generator output and the discharge impedance a Π-type network (modified Dressler VarioMatch 1000) was used to reduce capacitive coupling[24]. rf voltage, rf current and the phase between them is measured with high accuracy at the input side of the matching box (MKS Instruments VI-probe 4100).

The plasma chamber is pumped with a turbo molecular pump with Hohlweck stage to achieve a good compression also for H_2. The background pressure measured with an ionization gauge is of the order of 10^{-6} Pa. A butterfly valve in front of the turbo molecular pump allows to throttle the pumping speed. All experiments were conducted with a fixed butterfly position so that the residence time of the species was constant. The working pressure was always 1.0 Pa and was measured with a capacitance manometer before plasma ignition. The incoming gas flows are adjusted with mass-flow controllers. For the chosen butterfly position the required gas flows to achieve the working pressure of 1.0 Pa are $\Phi_{H_2} = 90$ sccm in case of pure H_2 and $\Phi_{Ar} = 50$ sccm for pure Ar (1sccm $= 4.48 \times 10^{17}$ particles per second). For different gas compositions the gas flow is varied in steps of $\Delta\Phi/\Phi_{max} = 20$ %, i.e., $\Delta\Phi_{Ar} = 10$ sccm and $\Delta\Phi_{H_2} = 18$ sccm. For the investigated H_2-Ar mixtures Ar gas flows of $x\Delta\Phi_{Ar}$ and H_2 gas flows of $(5-x)\Delta\Phi_{H_2}$ with $x = 1, 2, 3, 4$ were used. However, mass spectrometer investigations have shown that the flux ratios of Ar and H_2 are not identical to the partial pressure ratios for our experimental conditions. A differentially pumped mass spectrometer with cross-beam ion source was used to measure the actual partial pressures in the gas mixtures. The setup is described elsewhere[25,26]. It samples particles through an orifice at the outer diameter of the vessel in the central plane. In this work a carbon tube with a diameter of 600 μm and a length of 12 mm was used as orifice. The background pressure in the mass spectrometer chamber is of the order of 10^{-7} Pa. For a working pressure of 1.0 Pa in the plasma chamber the pressure in the mass spectrometer chamber raises for H_2

to 1.2×10^{-5} Pa and for Ar to 7.2×10^{-6} Pa. In addition, the mass spectrometer chamber is equipped with a shutter behind the orifice to allow distinguishing the isotropic background from the molecular beam that is formed. The particle density in this beam is proportional to the particle density in the vessel[27]. The beam component was obtained by subtracting the signal with closed shutter from the signal with opened shutter. The beam-to-background ratio R was measured and yields for Ar $R_{\mathrm{Ar}} = 5.0 \pm 0.3$ and for H_2 $R_{\mathrm{H_2}} = 1.5 \pm 0.1$.
In the following the procedure for determining the Ar fraction is described. A certain flow of a pure gas corresponds for the fixed butterfly position to a certain pressure in the main chamber. This main chamber pressure corresponds to a beam component measured with the mass spectrometer. The beam components of the mass spectrometer signals for the pure gases were calibrated against the pressure in the main chamber measured with the capacitive manometer. This calibration was made for the full partial pressure range applied in the experiments. The such calibrated mass spectrometer was in the following used to measure the partial pressures of the gas species in the gas mixtures. These measurements show that the partial pressure ratios for the gas mixtures are not identical to the gas flow ratios. This is most probably due to the pumping behavior of a gas mixture in the Knudsen flow regime if the gas species possess considerably different masses. A similar demixing has been observed earlier by Poschenrieder[28]. The Ar fraction is defined as $f_{\mathrm{Ar}} = p_{\mathrm{Ar}}/(p_{\mathrm{Ar}} + p_{\mathrm{H_2}})$ where p_{Ar} and $p_{\mathrm{H_2}}$ are the partial pressures measured with the mass spectrometer in the plasma-off state. This procedure yields the following Ar fractions for the above-mentioned flow ratios: 12.6, 28.0, 48.0, and 72.3 %. The total pressure p_{tot} of 1.0 Pa before plasma ignition stays constant during the discharge within the measurement accuracy of ± 2 %.

A combined energy and mass analyzer (Pfeiffer plasma process monitor PPM 422, Inficon AG Balzers) - in the following designated as plasma monitor (PM) - is incorporated into the upper, grounded electrode (see Fig. 1). The plasma monitor is twofold differentially pumped. Particles are sampled through two aligned orifices 100 and 500 μm in diameter, respectively. The two differential pumping stages assure a sufficiently low pressure in the plasma monitor system. For a working pressure of 1.0 Pa in the plasma chamber for H_2 a pressure of 7.7×10^{-6} Pa results in the plasma monitor and for Ar 1.1×10^{-6} Pa. The first orifice, which faces the plasma, is kept at ground potential. The second orifice separating the first and second pumping stage has a potential of -80 eV with respect to ground to attract positive ions. The plasma monitor consists of an Einzel lens (EL), an electron impact-

ionizer (IZ) to detect neutrals, a cylindrical-mirror energy analyzer (CMA), a quadrupole mass filter (QMS), and a Faraday cup (FC) arranged in series. There is also a secondary electron multiplier (SEM) as particle detector installed, but because of long term stability and reproducibility the FC was used in this study. A discriminator voltage V_{PM} accelerates or decelerates incoming ions to a constant pass energy in the energy filter of 15 eV corresponding to an energy resolution of $\Delta E_{\mathrm{PM}} = 0.8$ eV (full width at half maximum). The mass filter is operated at high mass resolution.

The plasma monitor measures either in the so called mass mode at a fixed discriminator voltage V_{PM} or in the so called energy mode at a fixed mass to charge ratio M_k of a species k (here only single charged ions are assumed). In this work the energy mode at a fixed mass M_k was used to measure the ion signals $S_{\mathrm{PM},k}(V_{\mathrm{PM}})$ as a function of the discriminator voltage V_{PM} with a step width of $\Delta V_{\mathrm{PM},s} = 0.063$ V. V_{PM} is related to the ion energy E_{ion} according to $eV_{\mathrm{PM}} = E_{ion} + eV_{\mathrm{PM},0}$ where $V_{\mathrm{PM},0}$ is an offset voltage and e is the elementary charge. The appropriate M_k was determined in a preceding mass scan. The signal S_{PM} is defined as the collected current I_{PM} measured with the Faraday cup at V_{PM} divided by the measurement step width $\Delta V_{\mathrm{PM},s}$.

The setup is equipped with a Langmuir probe that can be radially moved in and out of the plasma and axially between the two electrodes. The probe consists of a single cylindrical tungsten tip 3 mm in length and 50 μm in diameter. The reference electrode with a diameter of 8 mm is integrated in the probe head. To minimize the influence of the casing on the sheath around the tip a thin ceramic tube with a length of 5.5 mm and a diameter of 1 mm separates the casing from the tip. In addition, the front of the casing is covered with a ceramic coating. The reference electrode is equipped with a passive resonant rf compensation circuit. This floating reference electrode design is similar to the APS3 system[29]. I-V curves are acquired with the control and measuring unit PlasmaMeter[30,31]. For all measurements shown in this article the probe was positioned in the axial center of the discharge 2 cm above the quartz dome. The probe was cleaned by keeping the probe at high negative voltage (-100 V) for 10 s prior to the measurement procedure. No significant change of the measured Langmuir probe values was observed for measuring with and without cleaning. During measurements with the plasma monitor and optical emission spectroscopy the probe was retracted.

A planar retarding field analyzer (RFA) allows to measure mass-integrated ion energy distributions. The retarding field analyzer can be rotated around its axis and moved radially

in and out of the plasma as well as axially between the two electrodes. It samples ions through an orifice with a diameter of $d_{\mathrm{RFA}} = 1.5$ mm. Its four grid design follows the recommendations by Conway et al.[32]. To prevent the plasma from penetrating into the RFA a grounded gold mesh with 1000 lines/inch is placed directly behind the orifice. A second grid with 100 lines/inch and a potential of $\Phi = -54$ V is used to repel the electrons. On the third grid (100 lines/inch) the retardation voltage V_{RFA} is applied. The fourth grid with 100 lines/inch and $\Phi = -82$ V is used to prevent the escape of secondary electrons created on the collector plate ($\Phi = -73$ V) where the ions impinge to measure the current. The RFA measures ion fluxes as a function of V_{RFA}. The ion energy distribution can be obtained by differentiating the measured ion flux with respect to V_{RFA}. The geometrical transmission probability for the ions was determined to be $T_{\mathrm{RFA}} = 0.19$. The total ion flux is related to the measured current I_{RFA} at $V_{\mathrm{RFA}} = 0$ V by

$$j_{\mathrm{RFA}} = \frac{I_{\mathrm{RFA}}}{0.25\pi d_{\mathrm{RFA}}^2 \times e \times T_{\mathrm{RFA}}}. \tag{1}$$

The miniature RFA is designed for working conditions that do not require differential pumping. Therefore, the distance between the entrance orifice and the collector plate is 2.4 mm only. For the actual pressure of 1 Pa the mean free path of Ar^+ ions with 20 eV is 18 mm (with a total cross section considering elastic and charge exchange collisions of 4.7×10^{-19} m^2 and a gas temperature of 600 K) and therefore the influence of collisions should be small[33]. For hydrogen and helium the mean free paths are similar[33,34]. Measurements showed that below 1 Pa for all three gases the RFA delivers ion fluxes at $V_{\mathrm{RFA}} = 0$ V equal to those measured with the Langmuir probe. For increasing Ar pressure the total ion flux in the RFA decreases in spite of a constant or even increasing ion flux measured with the Langmuir probe. The same effect was also observed in Ref.[35] and an empirical correction was derived. Here we do not intend to correct for this effect but restrict ourselves to a maximum pressure of 1.0 Pa where the RFA ion flux measurement is still undisturbed. For hydrogen and helium the effect of a decreasing RFA flux for increasing pressure starts at even higher pressures as will be discussed in more detail later.

Optical emission spectroscopy (OES) was applied to measure the gas temperature and the dissociation degree of hydrogen. The light emitted from the plasma is collected by a lens after passing through a BK7 glass window separating vacuum from ambient-atmosphere and an aperture with a diameter of 1 mm. The emitted light is sampled along a line of sight

approximately 10 mm in diameter radially through the plasma 20 mm above the quartz dome. The light is collimated by an aperture with a diameter of 1 mm. A plano-convex lens focusses the light into a quartz fibre cable guiding it to a Czerny-Turner spectrograph (Acton SpectraPro 275) with a focal length of 275 mm. The entrance slit of the spectrometer has a width of 40 μm. The spectrometer is equipped with three exchangeable gratings with 150, 600 and 1800 lines per mm. All experiments were conducted with the 1800 l/mm grating, which has a measured resolution of 0.15 nm at $\lambda = 600$ nm. The light is detected by a CCD array (EEV 256x1024 OE CCD30, PIXIS, Princeton Instruments). A relative sensitivity calibration of the spectrograph was performed with a calibrated halogen lamp and D_2 arc discharge light source.

III. QUANTITATIVE DETERMINATION OF PLASMA PARAMETERS

A. Calibration process of the plasma monitor signals

In this section the procedure to transform measured signal intensities $S_{\mathrm{PM},k}$ for an ion species k into ion densities $n_{\mathrm{PM},k}$ is described. First, it is shown how the measured signals S_{PM} are related to the ion fluxes onto the orifice. To this end the detection efficiency is analyzed. Second, the relative fluxes are converted into ion densities. This conversion is carried out applying a simple sheath model and assuming an ion density profile inside the plasma. For the conversion we use the electron density n_e determined with the Langmuir probe together with the gas temperature T_g determined by spectroscopy (see Sect. III A 3).

1. Total detection efficiency of the plasma monitor

To measure absolute *ion fluxes* with the PM a total detection efficiency η_{PM} would be required. In this section we attempt to determine this experimentally. In general, η_{PM} is influenced by the properties of the incoming ion beam such as ion energy, ion density, angular distribution and ion mass which depend on the plasma conditions, e.g. plasma pressure, rf power and gas species composition. The complex set-up of the PM consisting of ion optics, cylindrical-mirror analyzer and quadrupole mass spectrometer does not allow to predict the dependencies a priori. Nevertheless, in the following we try to outline general trends. To determine the detection efficiency η_{PM} of the plasma monitor one would need a source of

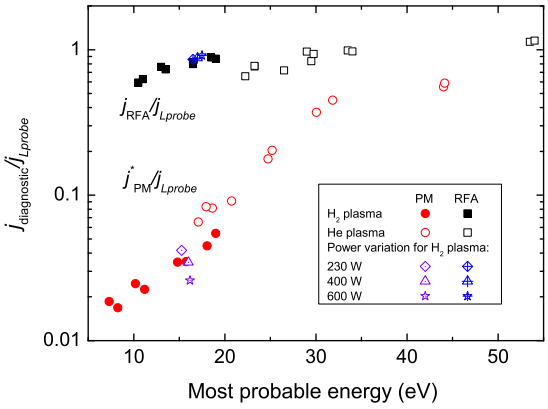

FIG. 2. PM and RFA fluxes j^*_{PM} and j_{RFA} normalized to the corresponding absolute ion flux j_{Lprobe} calculated from the Langmuir probe in pure H_2 and pure He plasmas. The power was varied to keep the electron density constant. The diamond, triangle and star indicate measurements for a constant H_2 pressure of 3 Pa and different rf powers, i.e., 230, 400 and 600 W.

ions with variable energy and known and variable flux as well as angular distribution which is experimentally nearly impossible (see also Ref.[36]). Ion energy distributions are measured with a plasma monitor by keeping the pass energy in the cylindrical-mirror analyzer constant to achieve constant energy resolution[37,38]. As a consequence, the CMA does not contribute to an energy-dependent effect. However, energy-dependent effects can arise from the limited acceptance angle of the system as well as from chromatic abberation due to the retardation or acceleration of the ions in the ion optics[39]. Space charge limitations can arise for higher densities or lower energies inside the PM. Ions can collide with the background gas while passing the plasma sheath as well as inside the PM. Mass-dependent effects can arise especially from the quadrupole mass spectrometer which is discussed in Sect. III A 2 in detail.

Here we attempted to characterize η_{PM} with a scan in plasma pressure and rf power for different gases. A change in pressure causes a change in electron temperature and consequently a change in the plasma potential and, hence, in the ion energy. However, if the pressure is varied also the plasma density changes. Therefore, we tried to keep the plasma density constant by rf power variation. In a second scan the rf power is varied at constant pressure to affect the plasma density but not the ion energy.

For the ion energy variation the pressure was changed between 1 and 6 Pa in He and between 2 and 7.5 Pa in H_2 plasmas. The electron density was maintained in the range $(5.5 \pm 1.5) \times 10^{15}\mathrm{m}^{-3}$ for the He plasma and $(1.8 \pm 0.1) \times 10^{16}\mathrm{m}^{-3}$ for the H_2 plasma by rf power variation.

Although we tried to keep the electron density constant a change in pressure causes the ion flux j to change. To account for that the total ion flux j_{Lprobe} can be calculated from n_e and T_e determined with the Langmuir probe. At the sheath edge the total ion flux is[19] $j_{Lprobe} = n_e \exp(-0.5)\sqrt{k_B T_e/M}$ where n_e and T_e are the electron density and temperature and M the ion mass.

To check if our approach with the pressure scan is valid we apply this method first to the RFA data. The RFA is a diagnostic where the detection efficiency is expected to be constant. It has due to its design a large acceptance angle and no chromatic abberation because of the absence of any ion optics. But the miniature RFA is not differentially pumped so that collisions inside the RFA volume are possible and have to be considered. For higher pressures, i.e., short mean free paths even the total current can be affected[35]. For the highest used pressure of 7.5 Pa the mean free path of H_3^+ in H_2 is 28 mm given a total cross section of 4×10^{-20} m^2 at 20 eV ion energy and 600 K gas temperature[33]. This mean free path is much larger than the dimensions of the RFA (2.4 mm from entrance orifice to collector plate) so that collisions can be neglected for hydrogen. Correspondingly, at 6 Pa the mean free path of He^+ ions in He is 2 mm given a total cross section[34] of 9×10^{-19} m^2. That means, for He collisions may affect the measurement for pressures higher than 5 Pa. $j_{\mathrm{RFA}}/j_{Lprobe}$ is shown in Fig. 2 as a function of the most probable energy. The most probable energy is the position where the ion energy distribution of the RFA is maximal. j_{RFA} is determined by Eqn. 1. The normalized RFA flux stays roughly constant within the accuracy of the measurements for both gases, He and H_2. The good agreement between He and H_2 is an indication that collisions do not yet play a role for these conditions. In addition, the absolute values of $j_{\mathrm{RFA}}/j_{Lprobe}$ are close to 1 indicating that the RFA and the Langmuir probe yield the same fluxes.

Next, the same procedure is applied to the plasma monitor measurements. He^+ and H_3^+ ion energy distributions are measured in the pure He and H_2 plasma, respectively. For the H_2 plasma H_2^+ and H^+ are neglected. This is justified because the PM measurements have shown that in this pressure range the contribution of H_3^+ to the total ion current is always

higher than 86 %. For the PM, the signal $S_{\mathrm{PM},k}$ is integrated over the discriminator voltage V_{PM}. The resulting value $j^*_{\mathrm{PM}} = \int S_{\mathrm{PM},k} dV_{\mathrm{PM}}/A_{\mathrm{PM}}$ is normalized by j_{Lprobe}. The area of the entrance orifice of the PM, A_{PM}, is taken into account to estimate the total ion flux into the PM, j^*_{PM}. $\eta_{\mathrm{PM}} = j^*_{\mathrm{PM}}/j_{Lprobe}$ represents the total detection efficiency of the plasma monitor. The results are also shown in Fig. 2 as function of the most probable energy. In contrast to the RFA measurements η_{PM} increases with increasing energy by more than one order of magnitude between 5 and 35 eV. For V_{PM} higher than 35 eV the slope of η_{PM} becomes smaller indicating saturation. The highest value of $\eta_{\mathrm{PM}} = 59$ % is surprisingly close to 100 % efficiency for these high energies. The reduction at low discriminator voltage we attribute to space charge limitations causing a change in the acceptance angle. However, the functional dependence of η_{PM} is in contrast to measurements by Pecher[40] who found a decrease proportional to $E^{-1.2}$. But it has to be mentioned that Pecher investigated electron cyclotron resonance plasmas at significantly lower pressures and used a plasma monitor of different type.

With a pressure scan not only the ion energy but also the mean free path length of ions and the sheath thickness change. If η_{PM} would be reduced by collisional effects then we would anticipate that values for H_2 are larger than values for He because the mean free path length for H_3^+ in H_2 is much larger than for He^+ in He as discussed above. This is not observed. Furthermore, collisions in the sheath would lead to a broader angular distribution of the ions entering the plasma monitor. If collisions in the sheath would be important we would anticipate that the ion energy distributions show a tail towards lower energy. For our conditions no such tail is observed (see Sect. IV F). So we conclude that also for the PM measurements collisions can be neglected.

To check the influence of plasma density on η_{PM} we varied the rf power for a H_2 plasma at 3 Pa. These data points are shown by the diamond, triangle and star symbols in Fig. 2. Three different rf powers were applied: 230, 400 and 600 W. The electron temperature and hence, the ion energy varies only slightly as expected for inductive discharges. The main effect is an increase in n_e from $1.1 \times 10^{16}\mathrm{m}^{-3}$ to $2.7 \times 10^{16}\mathrm{m}^{-3}$ as measured by the Langmuir probe. With increasing n_e also S_{PM} should increase and, therefore η_{PM} should stay constant. But as can be seen clearly in Fig. 2 this is not the case. With increasing rf power η_{PM} decreases. We attribute this deviation to space charge limitations inside the PM. This shows that even in this rather narrow parameter range the PM detection efficiency

is influenced not only by the ion energy but amongst other things also by the ion density. This clearly shows that a global detection efficiency η_{PM} for arbitrary plasma conditions cannot be determined. Therefore, it is in general not possible to compare quantitatively two plasma monitor signals $S_{\mathrm{PM},k}$ with each other, neither for different plasma conditions nor for different species k.

In the following we want to outline cases where it is at least possible to determine *relative fluxes*. These relative fluxes can then be either compared with each other or absolutely quantified by other plasma diagnostics. In other words, our approach is to decompose η_{PM} into independent functions of known parameters like the ion mass M or the energy E:

$$\eta_{\mathrm{PM}} = T_{md} \times T_{ed} \times .., \tag{2}$$

where T_{md} is the so-called mass-dependent transmission and T_{ed} is energy-dependent transmissions. To compare different species k for a fixed plasma condition the mass-dependent transmission $T_{md}(M)$ is required. To be able to compare for the same species different plasma conditions T_{ed} is needed.

The relative flux $j_{\mathrm{PM},k,rel}$ can then be expressed by:

$$j_{\mathrm{PM},k} \propto j_{\mathrm{PM},k,rel} = 1/T_{md}(M) \int_0^\infty 1/T_{ed}(V) \times S_{\mathrm{PM},k}(V_{\mathrm{PM}}) dV_{\mathrm{PM}}. \tag{3}$$

Commonly the PM raw signal is integrated over the energy (see, e.g., Refs.[16,18]). This implicitly assumes that T_{ed} is constant. If this assumption is not valid the integrated signal is not proportional to the individual ion flux $j_{\mathrm{PM},k}$ of an ion species k onto the orifice. Due to the fact that the correct IED for an investigated plasma is not known a priori, there exists no objective criterion that could be applied to optimize the ion optics settings using PM measurements only. In favorable cases, e.g., noble gas plasmas at relatively low pressures, it should be possible to determine T_{ed} from a comparison of RFA- and PM-measured IEDs. There are at least two articles[36,38] that discuss the fact that the transmission through a plasma monitor depends on the particle energy and that the energy-dependent transmission can change depending on the settings in the ion optics. For their studies they used a different plasma monitor system, namely a Hiden EQP 300 energy-resolved mass spectrometer. Both studies developed elaborate optimization procedures to measure the 'real' IED by finding parameter sets for the ion optics that produce a flat T_{ed}.

In our case the ion energy distributions for one plasma condition are similar in position and

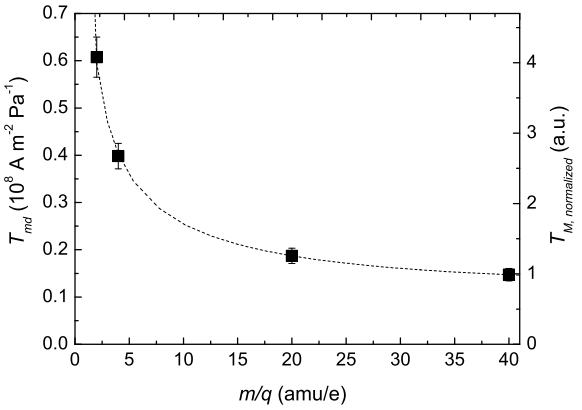

FIG. 3. Mass transmission of the plasma monitor obtained by neutral gas mass spectrometry. The right scale is normalized to the value of argon. The dotted line shows the regression curve according to Eqn. 7.

.

shape. In first order approximation only the height $h_{\mathrm{PM},k}$ of the curves varies with k. This implies that Eqn. 3 can be written as:

$$j_{\mathrm{PM},k,rel} \approx 1/T_{md}(M) \times h_{\mathrm{PM},k} \times \mathrm{const} \tag{4}$$

where the integral and, therefore,the unknown $\eta_{\mathrm{PM}}/T_{md}$ is included in the constant. Only if this assumption is valid PM signals can be converted to relative fluxes and compared with each other. These relative fluxes can in the following be normalized to the total flux to yield normalized values $j_{\mathrm{PM},k,norm}$:

$$j_{\mathrm{PM},k,norm} = \frac{j_{\mathrm{PM},k,rel}}{\sum_k j_{\mathrm{PM},k,rel}}. \tag{5}$$

By comparison with plasma diagnostics measuring absolute but mass-integrated ion fluxes, $j_{\mathrm{PM},k,rel}$ can be converted into absolute and mass-resolved fluxes $j_{\mathrm{PM},k}$.

2. Mass-dependent transmission

In general, mass-dependent effects can neither arise from the extraction nor from the electrostatic lenses but only from the quadrupole and/or the particle detector. In our case, we do not use a secondary electron multiplier but a Faraday cup. Because the Faraday

detector delivers mass-independent data the quadrupole remains here the only element that can show mass-dependent detection efficiency. The mass-dependent transmission was determined by neutral-gas mass spectrometry. This is valid as long as the kinetic energy of ions in the quadrupole is the same for the ions originating from the plasma or from the electron-impact ionizer in front of the PM's energy analyzer used for neutral gas analysis. Under this restriction the transmission measured with neutral-gas mass spectrometry can be transferred to plasma ions[40]. For measuring the mass-dependent transmission the plasma chamber is filled with a pure gas of species k with mass M_k at a pressure p_k without igniting a discharge. p_k is measured with an absolute pressure gauge. Because a beam is formed behind the extraction orifice the density in the ionizer of the PM is defined by molecular flow conditions and is therefore proportional to the pressure in the plasma vessel[27]. Dividing the signal $S_{\mathrm{PM}}(M_k)$ measured for this species by its neutral pressure p_k in the vessel and the partial cross section for electron-impact ionization $\sigma_{gas}(eV_e)$ at the used electron energy $eV_e = 70$ eV (σ_{gas} is taken from Ref.[41,42]) one obtains a signal that depends on the ion mass only[43]. For species were several isotopes are present the natural abundance α_k of the detected ion needs to be additionally taken into account. $T_{md}(M_k)$ then reads:

$$T_{md}(M_k) = \frac{S_{\mathrm{PM}}(M_k)}{\alpha_k \times p_k \times \sigma_k} \tag{6}$$

Figure 3 shows the experimental results for the mass-dependent transmission as a function of M_k for hydrogen, helium, neon and argon. For hydrogen only the H_2^+ ion which is produced by direct ionization is considered. H^+ is not taken into account because it is produced by dissociative ionization and will have excess kinetic energy that leads in general to a different transmission[44]. In addition, the right-hand scale shows the mass-dependent transmission $T_{M,\mathrm{normalized}}$ normalized to argon. One can see that $T_{M,\mathrm{normalized}}$ for H_2^+ is four times larger than for Ar^+ ions. In other words, neglecting this effect one would underestimate Ar by a factor of 4 when comparing directly signal intensities. The measured results are fitted to a regression curve $T_{md}^{fit}(M_k)$:

$$T_{md}^{fit}(M_k) = \frac{1}{\sqrt{-0.60242 + 1.74803 \times M_k - 0.01451 \times M_k^2}} \tag{7}$$

with a relative uncertainty $\Delta T/T$ of 10 % obtained from the regression curve. The regression curve is also shown in Fig. 3.

ion	H_2 (10^{-19} m^2)	Ar (10^{-19} m^2)
H^+	9.0	7.9
H_2^+	6.6	7.9
H_3^+	7.8	8.8
Ar^+	4.3	9.7
ArH^+	7.2	10.6

TABLE I. Used cross sections considering elastic and charge exchange collisions between an ion species k and neutral species H_2 and Ar taken from Ref.[33] for a gas temperature of 540 K.

In the last section we derived the prerequisites to calculate relative ion fluxes $j_{\mathrm{PM},k,rel}$. Only if these are fulfilled different ion species k can be quantitatively compared with each other. Together with an independent diagnostic such as a Langmuir probe or a retarding field analyzer relative fluxes can be converted to absolute fluxes.

3. Absolute densities

In this work we aim for ion densities. Therefore, the relative fluxes $j_{\mathrm{PM},k,rel}$ measured with the PM have to be converted to relative ion densities $n_{\mathrm{PM},k,rel}$. This is done by considering a simple sheath model where the ion flux is assumed to stay constant in the sheath. At the sheath edge (position x_0) the ion flux $j_{\mathrm{PM},k}$ of an ion species k can be expressed by the Bohm velocity $v_{B,k}$ and the ion density $n_{\mathrm{PM},k}(x_0)$:

$$j_{\mathrm{PM},k} = n_{\mathrm{PM},k}(x_0) \times v_{B,k}, \tag{8}$$

where $v_{B,k} = \sqrt{k_B T_e / M_k}$ with T_e being the electron temperature. According to Godyak the bulk ion density n_k can be related to the ion density at the sheath edge $n_{\mathrm{PM},k}(x_0)$ by a simple model[45] for cylindrical geometry as follows:

$$n_{\mathrm{PM},k} = \frac{n_{\mathrm{PM},k}(x_0)}{h_{l,k}}, \tag{9}$$

with $h_{l,k}$ given by:

$$h_{l,k} = \frac{0.86}{\sqrt{3 + \frac{l}{2\lambda_k}}}, \tag{10}$$

where l is the distance between the two electrodes and λ_k the mean free path defined by:

$$\frac{1}{\lambda_k} = \sum_j n_j \sigma_{k,j}. \tag{11}$$

$\sigma_{k,j}$ denotes the total cross section considering elastic and charge exchange collisions between an ion species k and neutral species j. $\sigma_{k,j}$ is taken from Ref.[33] for a gas temperature of 540 K (see OES results). Values for $\sigma_{k,j}$ are listed in Tab. I.

Inserting Eqns. 8 and 10 into Eqn. 9, yields for the individual ion density $n_{\mathrm{PM},k}$ in the bulk which is proportional to relative densities $n_{\mathrm{PM},k,rel}$:

$$n_{\mathrm{PM},k} \propto n_{\mathrm{PM},k,rel} = \sqrt{M_k}/h_{l,k} \times j_{\mathrm{PM},k,rel}. \tag{12}$$

Next, $n_{\mathrm{PM},k,rel}$ of all individual species k have to be summed up to yield the mass-integrated relative ion density $n_{\mathrm{PM},rel}$:

$$n_{\mathrm{PM},rel} = \sum_k n_{\mathrm{PM},k,rel}. \tag{13}$$

The final step to determine absolutely quantified ion densities $n_{\mathrm{PM},abs}$ is to normalize the result of Eqn. 13 with the Langmuir probe measurements. Quasi neutrality yields $n_e = \sum_k n_k$ and therefore the bulk electron density n_e can be used to determine the calibration constant C_{calib}:

$$n_{\mathrm{PM},abs} = C_{calib} \times n_{\mathrm{PM},rel} \equiv n_e. \tag{14}$$

It has to be kept in mind that this evaluation of PM intensities is valid only if T_{ed} and T_{md} are known (see Eqn. 3) and all other dependencies are constant for the investigated parameter range. If, e.g., T_{ed} is not known and the different ion species have different ion energy distributions no quantitative ion densities can be derived from the PM intensities. However, in cases where the ion energy distributions for the different ion species are comparable in position and shape in first order approximation normalized densities can be derived from the relative densities because the detection efficiency cancels out in the normalization step. The normalized densities are given by:

$$n_{\mathrm{PM},k,norm} = \frac{n_{\mathrm{PM},k,rel}}{n_{\mathrm{PM},rel}}. \tag{15}$$

4. Linearity and reproducibility of the plasma monitor

Due to the before-mentioned saturation effects of the PM signal at higher plasma densities, the linearity of the plasma monitor was tested in a separate set of experiments. A

Neon discharge was used because it has two isotopes with masses 20 and 22 amu with a ratio of the natural abundance $^{22}Ne/^{20}Ne$ of 0.102. This allows to test the linearity within one order of magnitude for one experiment. To extend this range pressure and rf power were adjusted to vary the signal intensity of Ne ions, $S_{\mathrm{PM,Ne}}$, by two orders of magnitude which is the considered intensity range for the final H_2-Ar measurements. The ratio $\tilde{S}_{\mathrm{PM},22}/\tilde{S}_{\mathrm{PM},20}$ for $^{22}Ne^+$ and $^{20}Ne^+$ was determined for these plasma conditions where $\tilde{S}_{\mathrm{PM}}$ denotes the signal integrated over the discriminator voltage. The measured mean value - averaged over the whole investigated parameter range - of the ratio is $< \tilde{S}_{\mathrm{PM},^{22}Ne}/\tilde{S}_{\mathrm{PM},^{20}Ne} >= 0.096$ with a standard deviation of 0.004. Taking T_{md} into account yields a value for this ratio of 0.101. We, therefore, conclude that the uncertainty of the intensity is better than 4 % in the considered range.

The reproducibility of the plasma monitor was checked by repeating the whole set for the H_2-Ar measurements with the same experimental settings on two consecutive days. The standard deviation of the relative changes of the individual plasma monitor signal heights determined from this comparison was 8 %.

B. Langmuir probe

The electron energy distribution function (EEDF), the electron temperature T_e and the electron density n_e were determined with a Langmuir probe system. Several methods are used to derive T_e and n_e from a measured current voltage characteristic (I/V-characteristic). The methods are taken from Lieberman and Lichtenberg[19]. Here the electron density is used as plasma density which is identical to the density of the positive charge carriers in the bulk plasma due to quasi neutrality. Typically I/V-characteristics were measured between -30 V and +40 V with an increment of 0.5 V.

The second derivative of the measured current I is proportional to the electron energy probability function (EEPF) $g_p(E)$:

$$g_p(E) = \frac{\sqrt{8m_e e}}{A_p e^2} \times \partial^2 I/\partial E^2, \tag{16}$$

with m_e being the electron mass and A_p the probe surface. The electron energy E is determined by $E = eV_{pl} - eV$. The plasma potential V_{pl} is defined by: $\partial^2 I/\partial E^2|_{V_{pl}} = 0$. The differentiation of the curve is combined with a smoothing technique as described in Ref.[31].

The curves are smoothed within a smoothing interval chosen to be 2 V in this work. The electron energy distribution function (EEDF) g_e is obtained by multiplying the EEPF with the square root of the electron energy.

The first method for the determination of the electron temperature, $T_{e,slope}$, is to use the reciprocal slope of the EEPF in the electron retardation regime. For this evaluation the low energy region is considered here (see also Fig. 6). The high energy region beyond the first kink could not be used due to increasing noise with increasing energy.

A second method to derive T_e and n_e uses directly the I/V-characteristic. T_e is calculated by the potential difference $\Delta V = V_{pl} - V_{fl}$, where V_{pl} denotes the plasma potential and V_{float} the floating potential. V_{fl} is defined as the voltage, where the probe current I vanishes. For a planar probe with collisionless sheath the electron temperature $T_{e,Vpl}$ is derived according to Lieberman and Lichtenberg[19]:

$$k_B T_{e,\Delta V} \;=\; \frac{2e\Delta V}{(lnM_{eff} \;-\; ln(2\pi m_e))}. \tag{17}$$

Here M_{eff} denotes the effective mass. M_{eff} has to be introduced for calculating the total ion flux $j_{i,tot}$ to the surrounding walls from the total ion density $n_{i,tot}(x_0)$ at the sheath edge if several ion species k are present in the plasma. The sum of the partial ion fluxes $j_{i,k}$ is set equal to the total ion flux $j_{i,tot}$:

$$j_{i,tot} = n_{i,tot}(x_0) \times \sqrt{\frac{k_B T_e}{M_{eff}}} = \sum_k j_{i,k}. \tag{18}$$

$j_{i,k}$ is equal to $n_{i,k}(x_0) \times v_{B,k}$ (see also Eqns. 8 and 9) where $n_{i,k}$ denotes the density of the ion species k. To derive M_{eff} from Eqn. 18 it is sufficient to know the relative mass-resolved ion fluxes $j_{\mathrm{PM},k,rel}$ or densities $n_{\mathrm{PM},k,rel}$ measured with the plasma monitor (see Sect. III A 3). Solving Eqn. 18 for M_{eff} yields (see also Ref.[20]):

$$\frac{1}{\sqrt{M_{eff}}} = \frac{\sum_k n_{\mathrm{PM},k,rel} \times h_{l,k} \times \frac{1}{\sqrt{M_k}}}{\sum_k n_{\mathrm{PM},k,rel} \times h_{l,k}} = \frac{\sum_k j_{\mathrm{PM},k,rel}}{\sum_k \sqrt{M_k} \times j_{\mathrm{PM},k,rel}}. \tag{19}$$

Eqn. 17 is based on a theory for planar probes but is used here also for the cylindrical probe. Furthermore, in Eqn. 17 the assumption is made, that the EEDF is a Maxwellian distribution which is, however, only a crude simplification for most cases and can deviate strongly from the real EEDF. For plasma conditions similar to the ones considered here, EEDFs with two regions of different slopes separated by a kink were observed[20]. Therefore,

this value for $T_{e,\Delta V}$ has to be used with care as will be discussed later.
The corresponding electron density n_e is calculated from the electron saturation current $I_{e,sat}$. $I_{e,sat}$ is defined as the current at $V = V_{pl}$ where all electrons can reach the probe. The electron density $n_{e,Iesat}$ is proportional to $I_{e,sat}$:

$$n_{e,Iesat} = \frac{I}{e\bar{v}_e A_p/4} = \frac{I_{e,sat}}{eA_p\sqrt{\frac{k_B T_{e,slope}}{2\pi e m_e}}}, \tag{20}$$

with A_p and $\bar{v}_e$ being geometrical probe surface and the mean velocity of the electrons in the plasma, respectively. Here $T_{e,slope}$ is used because this is the electron temperature of the low energy part of the EEPF where $I_{e,sat}$ is measured.

The third method to obtain n_e and T_e uses the moments of the EEDF[46]. This method is independent of a specific shape of the EEDF. $T_{e,eff}$ and $n_{e,\mathrm{EEDF}}$ are given by:

$$k_B T_{e,eff} = \frac{2}{3n_e}\int_0^\infty E \times g_e(E)\, dE. \tag{21}$$

$$n_{e,\mathrm{EEDF}} = \int_0^\infty g_e(E)\, dE \tag{22}$$

The results for the electron densities and temperatures determined with the different methods are discussed in section IV D and IV E.
For the absolute calibration of the ion densities measured with the plasma monitor (see Sect. III A 3) n_e calculated by Eqn. 22 was used. This method was chosen because it does not require determination of T_e and should, therefore, have the lowest uncertainty.

C. Optical emission spectroscopy

1. Signal evaluation

The measured signal $D(\lambda)$ (in arbitrary units) results from the emitted photons integrated along the line of sight through the plasma as a function of the wavelength λ in a time interval t_{int}. The signal was relatively quantified by multiplying with the relative sensitivity curve $R(\lambda)$ obtained for our experimental setting using a halogen lamp and D_2 arc discharge light source for calibration. The plasma can be considered as a light source with a certain length d_{plasma}. Radially resolved Langmuir probe measurements gave $d_{plasma} = 0.25$ m. To derive the experimental line intensity $\dot{N}$ of an emission line with the total line width $\Delta\lambda$ at the

wavelength λ_0 the integral is calculated:

$$\dot{N} \propto \frac{1}{t_{int} \times d_{plasma}} \int_{\lambda_0-\Delta\lambda/2}^{\lambda_0+\Delta\lambda/2} (D(\lambda) - D_{bg}(\lambda)) \times R(\lambda)\, d\lambda \tag{23}$$

where D_{bg} is the background signal which has to be subtracted.

2. Optical actinometry

OES was used in this work to determine the H density by actinometry. For optical actinometry normally a rare gas of known concentration is added to the plasma to quantify the unknown concentration of a molecular or radical species[47]. The emitted light of two neighboring emission lines, one from the actinomer—the added nobel gas—and one from the species of interest are measured. The density of the species of interest can be calculated from the emission line ratio, the known concentration of the actinomer, and a constant which includes the corresponding rate coefficients for direct excitation. Two conditions have to be fulfilled so that actinometry can be successfully applied: The excited state is predominantly populated through excitation by electron collisions from the ground state, and de-excitation is dominated by spontaneous emission. To improve accuracy the excitation energy of the two used emission lines should be comparable. In this work optical actinometry is used to determine the density of atomic hydrogen in H_2-Ar mixtures. It is, therefore, not necessary to add an actinomer because the gas mixture already contains Ar with a known concentration.

The model adopted here is the simple corona equilibrium[19]. In steady state electron-impact excitation is counterbalanced by deexcitation through spontaneous emission to energetically lower lying states of the atom:

$$n_1 \times n_e \times k_{1i} = n_i \times \sum_{m<i} A_{im}. \tag{24}$$

Here n_1 is the ground state atom density, n_e the electron density, k_{ji} the rate coefficient of the inelastic electron collision where the atom is excited from the ground state 1 into a higher state i and A_{im} the transition probability for spontaneous emission from the state i into the lower state m emitting at a wavelength λ_{im}. The line intensity $\dot{N}_{ij}$ is the number of emitted photons with a certain wavelength λ_{ij} arising from the transition from a state i to a lower state j which is irradiated per volume and time into the whole solid angle:

$$\dot{N}_{ij} = n_i \times A_{ij}. \tag{25}$$

The state i is populated with the density n_i. Eqns. 24 and 25 can be combined to:

$$\dot{N}_{ij} = \frac{n_1 \times n_e \times k_{1i} \times A_{ij}}{\sum_{m<i} A_{im}} = n_1 \times n_e \times k_{im}^{eff} \tag{26}$$

with the effective rate coefficient k_{im}^{eff}. The rate coefficient k_{1i} is calculated by $k_{1i} =< \sigma_{1i} v_e >$ where σ_{1i} is the corresponding cross section and v_e is the electron velocity. The mean value k_{1i} is a function of T_e.

For the hydrogen atom the H_β line at 486.1 nm is used. This line is due to direct excitation from the ground state and no influence of dissociative excitation exists (see below). Equation 26 yields for the H_β line of atomic hydrogen:

$$\dot{N}_{H_\beta} = n_H \times n_e \times k_{H_\beta}^{eff}. \tag{27}$$

n_H is the atomic H density. The effective rate coefficient is directly taken from Ref.[48]. For the Ar atom the line at 750.4 nm is used because this line is predominantly excited by direct excitation from the ground state[49]. Equation 26 then reads

$$\dot{N}_{Ar_{750}} = n_{Ar} \times n_e \times k_{Ar_{750}}^{eff}. \tag{28}$$

The cross section is taken from Ref.[50] and the rate coefficient is calculated by assuming a Maxwell distribution of the EEDF. The branching ratio $A_{ij}/\sum_{k<i} A_{ik}$ for this excited state is 1 (see for example Ref.[51]).

With Eqns. 27 and 28 and the measured line intensities $\dot{N}_{H_\beta}$ and $\dot{N}_{Ar_{750}}$ the atomic hydrogen density can be calculated. The ratio of the atomic, n_H, to molecular hydrogen density, n_{H_2}, which is called dissociation degree in the following, is given by:

$$\frac{n_H}{n_{H_2}} = \frac{\dot{N}_{H_\beta} \times k_{Ar_{750}}^{eff} \times n_e \times n_{Ar}}{\dot{N}_{Ar_{750}} \times k_{H_\beta}^{eff} \times n_e} \times \frac{1}{n_{H_2}} = \frac{\dot{N}_{H_\beta} \times k_{Ar_{750}}^{eff}}{\dot{N}_{Ar_{750}} \times k_{H_\beta}^{eff}} \times \frac{f_{Ar}}{1 - f_{Ar}}. \tag{29}$$

The ratio of the Ar density and the H_2 density is assumed to stay the same value as prior to plasma ignition. This assumption is fulfilled because the dissociation degree will turn out to be rather low and experimentally no pressure change is observed when plasma is switched on or off for the considered conditions. From Eqn. 29 it becomes clear that the atomic to molecular hydrogen ratio is proportional to the ratio of the experimentally derived line intensities. Thus it is sufficient to measure relative line intensity values because any scaling factor to absolute values cancels out. Furthermore, it is sufficient to measure the Ar to

H_2 pressure ratio, but not the absolute densities which would require determining the gas temperature. This, in turn, would add an additional uncertainty. In summary the n_H/n_{H_2} ratio can be determined from relative values which results in a much lower uncertainty than measuring absolute values.

The rate coefficients show a strong dependence on the electron temperature, but the ratio of $k^{eff}_{Ar_{750}}$ and $k^{eff}_{H_\beta}$ varies only slightly with T_e because the shape of the two corresponding cross sections and the threshold energies are similar. Here the measured $T_{e,\Delta V}$ is used as input for the rate coefficients. Another assumption which is implicitly made in Eqn. 29 is that the density profiles of atomic hydrogen and Ar are similar. However, this is not necessarily fulfilled for reactive species such as atomic hydrogen. For the production and loss of atomic hydrogen the dissociation of H_2 by electron collisions within the plasma volume and the loss at the chamber walls are important. In the region above the coil n_e and T_e have shown flat radial profiles. So the production rate of H in the plasma volume can also be assumed to be constant over that region. Outside the plasma volume the H density will decrease due to wall losses and deviate from the Ar density. But because in this region the plasma density also decreases it does not significantly contribute to the emission of the H_β and Ar_{750} lines. Therefore, we assume that this effect does not markedly influence the measured H atom density.

To justify the application of the corona equilibrium (see Eqn. 24) a simple collisional radiative model for the excited hydrogen atom with the principal quantum number $n = 4$ is considered. Two competing processes to populate this excited state are assumed[20]. First, direct excitation of the hydrogen atom from the ground state by inelastic electron collision with the rate coefficient k_1 and, second, dissociative excitation of the hydrogen molecule by inelastic electron collision producing an excited H atom, a H atom in the ground state and an electron with the rate coefficient k_2. The corresponding rates are $R_1 = n_e n_H k_1$ and $R_2 = n_e n_{H2} k_2$. This leads to the condition that $n_H/n_{H2} \gg k_2/k_1$. To justify the assumption on which equation 24 is based k_1 should be much larger than k_2. As it will be shown in the results section, n_H/n_{H2} is of the order of 2 % and T_e for Ar containing plasmas varies between 3 and 5 eV. The ratio between k_2/k_1 for electron temperatures of 3 and 5 eV is 0.0013 and 0.0026, respectively[52]. So the condition $n_H/n_{H2} \gg k_2/k_1$ is fulfilled for the considered plasma. For our experimental conditions other effects such as quenching or reabsorption can be neglected due to the low pressure.

The error for the dissociation degree (Eqn. 29) consists of three contributions. The first is the signal error $\Delta D(\lambda) \leq 10$ % which was estimated by repeating the measurement series once. The second is the uncertainty and the radial variation of the electron temperature which affects the uncertainty of the ratio of the rate coefficients $\Delta(k^{eff}_{\mathrm{Ar}_{750}}/k^{eff}_{\mathrm{H}_\beta})(\Delta T_e) \leq 13$ %. The last uncertainty comes from the error of the calibration curve $R(\lambda)$ where $\Delta R(\lambda_{\mathrm{H}_\beta})/R(\lambda_{\mathrm{Ar}_{750}}) \leq 15$ A total uncertainty of 22 % was obtained by Gaussian error propagation.

3. Gas temperature

The H_2 gas temperature T_g is estimated by the rotational temperature T_{rot} of the H_2 molecule. This is derived from the relative line intensity distribution of the first 5 rotational lines $Q_1 - Q_5$ in the vibronic band $v' = v'' = 2$ (in the following denoted as V_2) of the Fulcher-α transition ($d^3\Pi_u - a^3\Sigma_g^+$). Some assumptions have to be made to relate the gas temperature to the population of the $d^3\Pi_u$ state. The upper level is assumed to be populated only by direct electron excitation from the electronic ground state $X^1\Sigma_g^+$ with $v = 0$ which does not change the rotational distribution. This condition is satisfied in low-pressure discharges[53,54]. The rotational distribution of the ground state is assumed to be thermally populated due to collisions with other gas particles.

Fantz[55] compared the experimentally obtained rotational temperature from the here considered Fulcher-α transition with the rotational temperature from the molecular nitrogen transition $C^3\Pi_u(v' = 0) \rightarrow B^3\Pi_g(v'' = 2)$ in a hydrogen-helium microwave plasma with an addition of a small amount of nitrogen in the pressure range between 10 and 100 Pa. It has been shown elsewhere that the rotational temperature of the N_2 $C^3\Pi_u$ state is equal to the gas temperature[56,57]. The result of Fantz[55] is that the temperature in the vibronic band V_2 of the Fulcher-α transition matches best with the nitrogen rotational temperature. Investigations of additional vibrational systems V_0, V_1 and V_3 revealed that the V_3 system yields a comparable but slightly lower rotational temperature while the other two yield significantly higher temperatures. The observed differences decrease with decreasing gas pressure. We, therefore, take the rotational temperature from the Fulcher-α V_2 transition as an estimate for the gas temperature.

A short description for the determination of T_{rot} based on Ref.[53,54] is given in the following. In general, the line intensity $\dot{N}^{p'v'J'}_{p''v''J''}$ of a transition is the product of the population density

$n^{p`v`J`}$ of the upper state times the transition probability $A^{p`v`J`}_{p``v``J``}$. Within one vibrational transition $v` \rightarrow v``$ of an electron transition from the upper state $p`$ (here $d\ ^3\Pi_u$) to the lower state $p``$ (here $a^3\Sigma_g^+$) the only variables that depend on the upper quantum number $J`$ are the statistical weight $\gamma_{J`}$ and the Hönl-London factor $S_{J`}$, the wavelength $\lambda^{p`v`J`}_{p``v``J``}$ and the rotational energy $E^{J`}$. The line intensity is then proportional to:

$$\dot{N}^{p`v`J`}_{p``v``J``} \propto (\lambda^{p`v`J`}_{p``v``J``})^{-3} \times \gamma^{J`} S^{J`} \times \exp(-\frac{E^{J`}}{k_B T^{v`=2}_{rot}(d^3\ \Pi_u)}). \tag{30}$$

Here $E^{J`}$ is the energy referenced to the $J` = 1$ state and taken from Ref.[58]. Values for $E^{J`}$, $S_{J`}$ and $\gamma_{J`}$ are summarized in Tab. II. After taking the logarithm of Eqn. 30 this yields

$$\ln(\frac{\dot{N}^{p`v`J`}_{p``v``J``}(\lambda^{p`v`J`}_{p``v``J``})^3}{\gamma^{J`} S^{J`}}) = -\frac{\Delta E^{J`}}{k_B T^{v`=2}_{rot}(d^3\ \Pi_u)} + \text{const.} \tag{31}$$

Plotting the value of the left hand side of Eqn. 31 as a function of the rotational energy difference $\Delta E^{J`} = E^{J`} - E^{J`=1}$ in the upper excited electrical state $d^3\Pi_u$ for the vibronic state $v` = 2$ yields a straight line. The reciprocal of the slope of this line is the rotational temperature of the excited state $T^{v`=2}_{rot}(d^3\ \Pi_u)$. The rotational population distribution of the ground state is related to the rotational population distribution of the excited state as:

$$T^{v=0}_{rot}(X^1\Sigma_g^+) = \frac{B_{v=0}(X^1\Sigma_g^+)}{B_{v`=2}(d^3\ \Pi_u)} T^{v`=2}_{rot}(d^3\ \Pi_u). \tag{32}$$

Here $B_{v=0}(X^1\Sigma_g^+)$ and $B_{v`=2}(d^3\Pi_u)$ denote the rotational constants of the lowest vibrational level of the ground state and from the vibrational level $v` = 2$ of the excited state $d^3\Pi_u$, respectively. In this work a $B_{v=0}(X^1\Sigma_g^+)/B_{v`=2}(d^3\ \Pi_u)$ of 2.24 is used[59].

Unfortunately, we observed additional emission lines around Q_4 when Ar was added to the H_2 plasma that overlap with Q_4. As in Ref.[54] Q_5 tends to deviate from the straight line even for pure H_2. Therefore, for the H_2-Ar mixture only the first three lines Q_1 to Q_3 were used for determining T_{rot}.

IV. RESULTS AND DISCUSSION

In the following we present the results for the gas temperature, the electron temperature and density, the effective mass, the ion densities and the dissociation degree.

A total pressure of 1.0 Pa was chosen as working pressure because of two reasons: First it is the minimum pressure where a pure H_2 plasma operates stably in the inductively coupled

Lines	$\Delta E^{J`}$ (cm^{-1})	$S^{J'}$	$\gamma^{J'}$	λ (nm)
Q_1	0	0.75	3	622.48
Q_2	117.77	1.25	1	623.03
Q_3	293.27	1.75	3	623.84
Q_4	525.13	2.25	1	624.92
Q_5	811.57	2.75	3	626.25

TABLE II. Rotational parameters for the $Q1$ to $Q5$ lines of the vibrational band $v` = v`` = 2$ of the $d^3\Pi_u$ state of H_2 taken from Ref.[54,58].

mode in our set-up. At lower pressure the plasma operates in the capacitively coupled mode where a drastic reduction in light emission and electron density accompanied by an increase in sheath thickness occurs. Second, for pure Ar plasmas and pressures above 3 Pa the results of the plasma monitor and the Langmuir probe started deviating from each other which we attribute to effects described in detail in Sect. III A 1 in the context of the detection efficiency of the PM. Because we aim for reliable, absolutely quantified results we do not present here systematic pressure and power scans, but restrict ourself to a scan of f_{Ar} at fixed total pressure.

In principle, the experiments with varying f_{Ar} can be performed in two ways. In the most simple case, f_{Ar} is varied keeping all other experimental parameters constant. Performing the experiment in this way it turned out that for constant rf input power the electron density varied by a factor of 12. We, therefore, decided to perform the experiments such, that we adapt the rf power in such a way that a variation in n_e is minimized as will be shown in section IV E. Because the electron density is not a simple control parameter for the experiment we chose the compromise to vary the rf input power between 500 W for a pure H_2 plasma and 100 W for a pure Ar plasma (see Fig. 4). As a result, n_e remains in a range of 3×10^{16} $m^3 \pm 20$ % if f_{Ar} is varied between 12.6 and 100 %. For the pure H_2 plasma n_e decreased by $\sim$65 %.

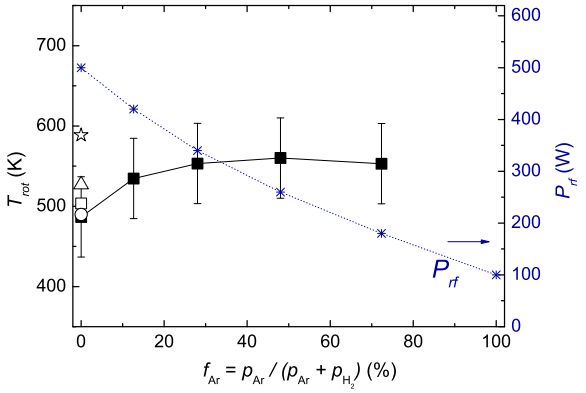

FIG. 4. Rotational temperature T_{rot} of the H_2 molecule (left-hand scale) and corresponding rf power (right-hand scale) as a function of f_{Ar} for a total pressure of 1.0 Pa. The solid symbols are derived from the rotational lines $Q_1 - Q_3$ for the vibrational transition V_2. The open symbols are derived from the rotational lines $Q_1 - Q_4$ for the vibrational transitions V_0 (star), V_1 (triangle), V_2 (square), and V_3 (circle).

A. Gas temperature

The rotational temperature T_{rot} of the hydrogen molecule is plotted in Fig. 4. The solid symbols are derived from the rotational lines $Q_1 - Q_3$ for the vibronic band V_2 (see Sect. III C 3). According to the data T_{rot} does not vary significantly with increasing Ar fraction. The mean value over the Ar fraction range from 0 to 72.3 % is 540 K. To asses the accuracy of the evaluation procedure values considering the $Q_1 - Q_4$ lines were computed for the pure H_2 plasma for V_2 as well as for V_0, V_1 and V_3 (open symbols) which were determined in analog manner to V_2 described in Sect. III C 3. T_{rot} decreases from 590 to 490 K for increasing vibrational transition V_i. This is in qualitative agreement with results of Fantz[55]. There, an even larger spread was observed. This spread decreases from 400 to 200 K with decreasing the pressure from 50 to 10 Pa. It is fair to assume that for further decreasing pressure this spread decreases even more. In that sense, the observed spread in our data of 100 K is in reasonable agreement with the data of Fantz[55]. From the difference in $V_0 - V_3$ values we estimate an uncertainty of 50 K for the gas temperature measurement. Accordingly, we use $T_g = T_{rot} = (540 \pm 50)$ K in the following.

T_g is influenced by the following heating mechanisms: momentum transfer between electrons

and neutrals, ion-molecule collisions and in the case of molecular gases also by dissociation and rotational excitation[56]. We estimate the dominant heating mechanism based on a simple model[56]. The cross sections for the individual processes are taken from Yoon et al.[60]. The evaluation shows that for our conditions and for a hydrogen plasma dissociation is the most important heating mechanism. As will be shown in Sect. IV B the dissociation degree turned out to be constant with varying f_{Ar} up to 72.3 %. So one would expect that T_{rot} also stays constant. In that sense, the observed constant T_{rot} seems reasonable.

In inductively coupled H_2-Ar mixtures no experimental results about T_g can be found in the literature to the knowledge of the authors. Kimura and Kasugai[20] and Hjartarson et al.[21] assumed for their rate equation modeling a T_g of 400 K and 500 K, respectively. In an inductively coupled pure Ar plasma Kiehlbauch et al.[61] simulated the gas temperature T_g resulting in $T_g \approx 600$ K at a pressure of 1.3 Pa and a power of 160 W. This was confirmed by measurements of Tonnis et al.[62] at slightly higher pressures. In a microwave H_2 and H_2-Ar plasma at a power of 600 W Tatarova et al.[63] measured T_{rot} from the Q branch of the Fulcher-α rotational spectrum ($v' = v'' = 0$). For the H_2 plasma T_{rot} varied between 500 and 600 K. For the H_2-Ar plasma with an Ar fraction of 90 and 95 % T_{rot} varied between 350 and 400 K. In their case Ar admixing led to a lowering of the dissociation degree. The lower T_{rot} in the mixture could therefore be due to a lower dissociative heating. Furthermore, in a He-H_2 plasma T_{rot} was compared to the Doppler temperature of He[63]. From the agreement of both the authors concluded that T_{rot} is an indicator of T_g as assumed in Sect. III C 3. In conclusion, the measured T_{rot} seems to be reasonable in comparison with the existing literature.

B. Dissociation degree

The dissociation degree of hydrogen is shown in Fig. 5. It was derived by actinometry via the ratio of the H_β/Ar_{750} lines as described in Sect. III C 2. The dissociation degree stays nearly constant over the considered Ar fraction range with a mean value of 1.7 ± 0.4 %. For the pure H_2 plasmas it was not possible to do actinometry so there were no data obtained and in the pure Ar plasma no H is present. Also shown in Fig. 5 is the absolute atomic hydrogen density n_{H} calculated with a gas temperature of 540 K. It decreases linearly with decreasing H_2 content from 2.3×10^{18} m^{-3} to 6.7×10^{17} m^{-3} for $f_{\mathrm{Ar}} = 12.6$ to 72.3 %.

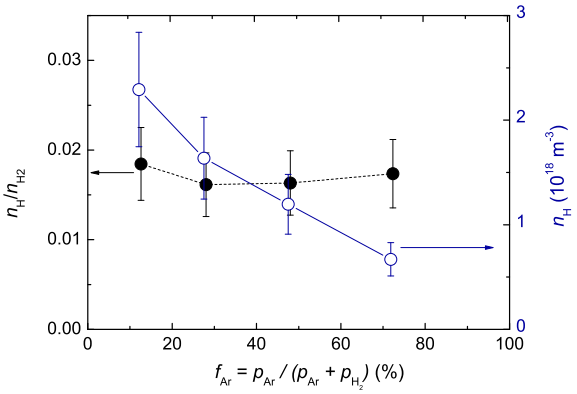

FIG. 5. Measured dissociation degree of hydrogen and absolute atomic density obtained with actinometry as a function of f_{Ar} for a total pressure of 1.0 Pa.

Knowing the absolute atomic hydrogen n_{H} density and the ion densities n_k in the plasma the atomic to ion flux ratio j_{H}/j_i can be calculated. j_{H} is expressed by the particle flux into a half space with a Maxwellian velocity distribution. j_i is the total ion flux to the surface (see Eqns. 8 and 9). So $j_{\mathrm{H}}/j_{i,tot}$ yields:

$$\frac{j_{\mathrm{H}}}{j_{i,tot}} = \frac{0.25 \times n_{\mathrm{H}} \times v_{\mathrm{H}}}{\sum_k h_{l,k} \times n_k \times v_{B,k}}. \tag{33}$$

In the following this ratio is estimated for a pure H_2 plasma. A dissociation degree of 1.7 % is assumed so the atomic hydrogen density is $n_{\mathrm{H}} = n_{\mathrm{H}}/n_{\mathrm{H_2}} \times p/(k_B T_g) = 2.0 \times 10^{18}$ m^{-3}. For the determination of the atomic hydrogen velocity the temperature T_{H} is assumed to be 3000 K which is based on measurements of Tatarova et al.[63]. There the atomic hydrogen temperature was measured in H_2 microwave plasmas at 30 Pa. It was shown that T_{H} lies between the half of the dissociation energy (2.2 eV) and the gas temperature (600 K). The atomic hydrogen mean velocity is estimated to 8.0×10^3 ms^{-1}. This results in an atomic hydrogen flux of 4.5×10^{21} m^{-2}s^{-1}. $j_{i,tot}$ in the pure H_2 plasma is 4.4×10^{19} m^{-2}s^{-1} calculated with Eqn. 18 and values taken from Sect. IV H. So the atomic to ion flux ratio yields $j_{\mathrm{H}}/j_{i,tot} = 102$. Manhard et al.[64] measured an ion flux of 1.3×10^{19} m^{-2}s^{-1} in an electron cyclotron resonance deuterium plasma for 1 Pa and 144 W microwave input power. Furthermore, they estimated the atomic deuterium flux to be in the order of 1×10^{21} m^{-2}s^{-1} resulting in an atomic to ion flux ratio of about 100. Their estimate is, therefore, in reasonable agreement with our results.

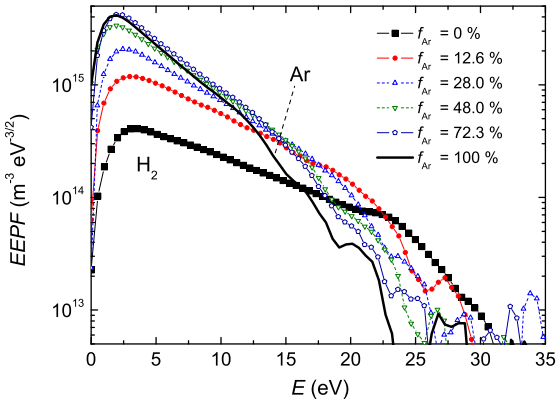

FIG. 6. Electron energy probability functions (EEPF) for various Ar fractions as determined by Langmuir probe measurements for a total pressure of 1.0 Pa. The curves are smoothed within a smoothing interval chosen to be 2 V.

The measured dissociation degree is considerably lower than the measurements and simulations from Kimura and Kasugai[20] where $n_{\mathrm{H}}/n_{\mathrm{H2}ploff}$ was about 25 % (here $n_{\mathrm{H2}ploff}$ denotes the gas density of H_2 during the plasma off state) for a pressure of 2.7 Pa, an absorbed power of 120 W, a similar vessel geometry and an Ar fraction of 50 %. For the considered pressure range the atomic H density depends sensitively on the surface loss probability for H loss at the surrounding walls[20,21,65,66]. For the simulations Kimura and Kasugai used a surface loss probability of 0.02. Hjartarson et al.[21] also assumed a surface loss probability of 0.02 for atomic hydrogen on stainless steel. Simulations with increasing surface loss probability from 0.02 to 1 showed a decrease of the dissociation degree by more than one order of magnitude. A possible explanation for the different dissociation degree between the present study and Kimura and Kasugai is that the surface loss probability in the present case is higher than in the experiment by Kimura and Kasugai.

C. Electron energy probability function

Figure 6 shows electron energy probability functions in H_2-Ar mixed plasmas with different f_{Ar} in form of a semi-logarithmic plot for p_{tot}=1.0 Pa. All distributions show a maximum at around 2-3 eV. The height of this maximum increases with increasing f_{Ar}. This change

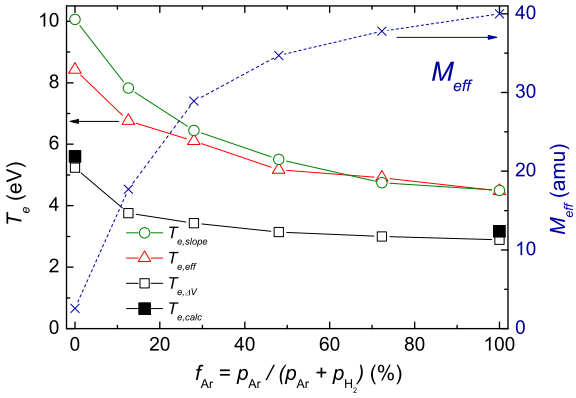

FIG. 7. Electron temperature T_e as a function of f_{Ar} (left-hand scale) for a total pressure of 1.0 Pa. Three methods were used to derive T_e. Furthermore, $T_{e,calc}$ calculated by a simple rate equation model is shown by a closed square for the pure H_2 plasma and the pure Ar plasma. The effective mass for the H_2-Ar plasma is also plotted (right-hand scale).

reflects the increase in electron density which can be determined from the integral of the EEDF (see Eqn. 22). None of the distributions is Maxwellian, but all consist of two distinctively different regions which are separated by a clear kink. The position of this kink drops monotonically from 22 eV for a pure H_2 plasma to 12 eV for a pure Ar plasma. The low energy regions of the EEPFs between the maximum and the first kink are characterized by smaller slopes compared to the high energy regions above the kink. EEPFs with two distinct regions with different slopes can be approximated by a bi-Maxwellian distribution with two distinct electron temperatures, e.g. as observed by Kimura and Kasugai[20]. Unfortunately, the high energy part can due to the high experimental noise not be attributed reliably to an electron temperature. Consequently, only the low-energy part is evaluated. For the data shown in Fig. 6 we find with increasing f_{Ar} a decreasing $T_{e,slope}$.

D. Electron temperature

The electron temperatures, evaluated using the three different methods described in Sect. III B, are plotted in Fig. 7. All three curves show a similar behavior. They decrease monotonically with increasing Ar fraction. $T_{e,slope}$ and $T_{e,eff}$ decrease from 10.1 and 8.4 eV

for f_{Ar} =0 % to 4.5 eV for f_{Ar} =100 %. The strongest decrease occurs between 0 and 12.6 % Ar fraction. The curve of $T_{e,slope}$ lies above $T_{e,eff}$ for low f_{Ar}. Above Ar fractions of 48 % the two different methods yield practically identical T_e values. In contrast, $T_{e,\Delta V}$ results in significantly lower electron temperatures for all conditions. $T_{e,\Delta V}$ decreases from 5.2 eV for 0 % Ar fraction to 2.9 eV for 100 % Ar fraction.

The effective mass as derived from the PM measurements, which is necessary to determine T_e according to Eqn. 17, is also presented in Fig. 7. M_{eff} increases with increasing Ar content. The increase is monotonic but not linear. M_{eff} increases faster for low Ar fractions than for high Ar fractions. Again the major increase occurs between a pure H_2 plasma and $f_{Ar} = 12.6$ %. The increasing effective ion mass is due to an increase in the ArH^+ and Ar^+ densities by a simultaneous decrease in the H_3^+ density for increasing f_{Ar} as will be shown in Sect. IV H.

For a similar type of discharge Hjartarson et al.[21] calculated the electron temperature for the plasma studied by Gudmundsson[17]. They found a decrease from 6 eV to 3.4 eV when changing from a pure H_2 plasma to a pure Ar plasma at a pressure of 0.93 Pa. These values are much closer to the $T_{e,\Delta V}$ values determined here than $T_{e,slope}$ and $T_{e,eff}$.

A simple rate equation model for one ion species[19] can provide additional arguments to asses which T_e value is more trustworthy. For the pure plasma case with only one dominant ion species particle conservation is used to derive the electron temperature:

$$\frac{\partial n_i}{\partial t} + \nabla \times \mathbf{\Gamma} = G - L, \tag{34}$$

where n_i is the ion density, $\mathbf{\Gamma} = n_i \mathbf{v}$ describes the ion flux to the wall, $\mathbf{v}$ is the ion velocity, and G and L are the rates for ion gain and loss processes in the plasma volume, respectively. The rate for the ion gain process (ionization: e + g $\rightarrow$ g^+ + 2e with e - electrons, g - background gas in the plasma, g^+ - ion species from g) is $G = n_e n_g k_{iz}$ (n_e - electron density, $n_g = p/(k_B T_g)$ - neutral gas density, p - neutral gas pressure, k_B - Boltzmann constant, T_g - neutral gas temperature, k_{iz} - ionization rate coefficient). The rate for the ion loss process (wall loss: g^+ + wall $\rightarrow$ g) is given by the wall flux $\mathbf{\Gamma} = n_i \mathbf{v}$ divided by an effective length d_{eff}. d_{eff} is the ratio of the discharge volume to the effective area for particle loss, which depends on the ratio of the ion density at the sheath to the ion density in the plasma center (Eqn. 10) and is a function of the ion mean free path length of the considered ion through the neutral gas. Here an effective loss area for the ions of $2\pi r^2 h_l$ (r - radius, h_l - ion

density ratio between sheath edge and plasma center, see Sect. III A 3) is assumed because the plasma is limited by the lower and upper electrode with a distance of $l = 60$ mm and a diameter of $2r = 131$ mm. Radial loss is neglected because $r > l$. Under the assumption of quasi-neutrality $n_e = n_i$ and after separating the quantities by their dependence on the electron temperature[19] Eqn. 34 yields:

$$\frac{k_{iz}(T_e)}{\sqrt{k_B \times T_e}} = \frac{1}{\sqrt{M_i} \times n_g \times d_{eff}}. \tag{35}$$

For Ar the neutral and ion species are the Ar atom and the Ar^+ ion, respectively. k_{iz} is calculated from the corresponding cross section, taken from Ref.[42] under the assumption of a Maxwellian energy distribution of the electrons. Eqn. 35 yields for a pure Ar plasma with a gas temperature of 540 K, an ion mass of 40 amu and a d_{eff} of 0.092 m a T_e of 3.2 eV. For the pure H_2 plasma case the hydrogen molecule is ionized by inelastic electron impact to form H_2^+ ($e + H_2 \rightarrow H_2^+ + 2e$). This ion species is quickly transformed by collisions with the neutral molecular hydrogen to H_3^+ ($H_2^+ + H_2 \rightarrow H_3^+ + H$), whose main loss channel is the flux to the wall ($H_3^+ + \text{wall} \rightarrow H + H_2$)[21]. So in Eqn. 35 the ion species is the H_3^+ and the neutral one is the H_2 molecule and k_{iz} is the rate coefficient for ionization of H_2 calculated from the corresponding cross section, taken from Ref.[60] again under the assumption of a Maxwellian energy distribution of the electrons. For a pure H_2 plasma with a d_{eff} of 0.086 m this yields a T_e of 5.6 eV. A comparison of Eqn. 35 for a pure Ar and a pure H_2 plasma at $p = 1.0$ Pa shows that only the ion mass changes markedly. With increasing ion mass, the value on the right-hand side of Eqn. 35 decreases. This can be counterbalanced by a decrease in T_e because the ionization rate coefficient decreases monotonically with T_e. This simple model does not only explain the trend but also quantitatively the difference between pure H_2 and Ar plasmas. Because $T_{e,\Delta V}$ is close to the values derived from this simple model, we assume that the electron temperature $T_{e,\Delta V}$ is more reliable than $T_{e,eff}$ and $T_{e,slope}$.

In general, the variation of T_e as a function of f_{Ar} is in good agreement with published data from Kimura and Kasugai[20]. They also attributed two electron temperatures to their EEPF which differ by a factor of 1.5. Their absolute values are lower than ours because of the higher pressure used in their experiments.

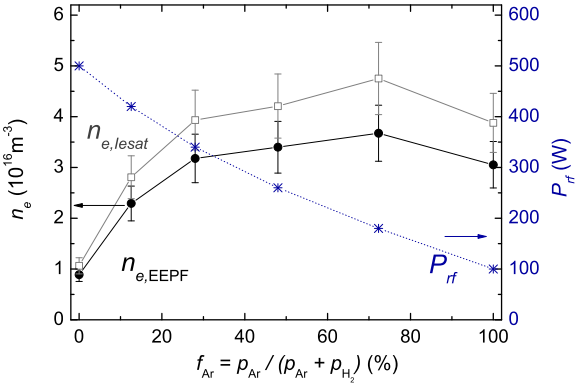

FIG. 8. Electron density n_e as a function of the Ar fraction for a total pressure of 1.0 Pa. Two methods were used to derive n_e, see Eqns. 20 and 22. The rf input power (right-hand scale) was varied in an attempt to minimize the variation in electron density.

E. Electron density

The electron density is derived by two methods as described in Sect. III B. The results are shown in Fig. 8 together with the rf input power. $n_{e,\mathrm{EEDF}}$ from Eqn. 22 is about 20 % lower than $n_{e,Iesat}$. The shapes of the two curves are very similar. This indicates that the relative uncertainty of n_e is low. In both cases n_e increases by a factor 3-4. However, there is an uncertainty in the absolute scale of n_e due to uncertainties in the absolute values of $I_{e,sat}$ and A_p. It has to be kept in mind that the rf input power P_{rf} is varied in an attempt to minimize the variation in n_e. Nevertheless, at low Ar fractions the electron density increases by a factor of 3 from $f_{\mathrm{Ar}} = 0$ % to 28 % and stays roughly constant around 3 to 4×10^{16} m^{-3} in the region for $f_{\mathrm{Ar}} \geq 28$ %. Without rf power variation n_e would increase by a factor of 12.

Comparing electron density and rf power between different experimental setups is difficult due to complicated rf coupling efficiency. As a consequence the correlation between forwarded rf power, discharge geometry and electron density remains a specific property for each discharge setup. In the work of Gudmundsson[17] n_e increases exponentially with increasing Ar fraction from 2.5×10^{16} m^3 for $f_{\mathrm{Ar}} = 15$ % to 3×10^{17} m^3 for the pure Ar plasma ($p = 0.9$ Pa, $P = 600$ W). Kimura and Kasugai[20] measured n_e for a pressure of 2.7 Pa and a constant power of 120 W. They found that n_e increases for increasing f_{Ar} from

5×10^{16} m^3 for $f_{\mathrm{Ar}} = 50$ % to 4.5×10^{17} m^3 for a pure Ar plasma. In our experiments we observed a comparable increase of the plasma density with f_{Ar} if the applied rf power is held constant. These three experimental observations are in reasonable agreement with each other and prove the general trend that in H_2-Ar plasmas n_e strongly increases with increasing argon fraction for constant applied rf power.

A global model[19] using the energy balance equation delivers a relation between P_{rf} and n_e. P_{rf} is proportional to the electron density times the total energy loss per electron-ion pair lost from the system. This is dominated by the collisional energy loss E_c per electron-ion pair created. For atoms the energetic loss channels are due to ionization, excitation to electronically excited states and elastic scattering of electrons with the atoms. For molecules dissociation and excitation of vibrational and rotational energy levels contribute additionally. As a consequence for molecular gases higher power for the same electron density is needed. A comparison of E_c between Ar and H_2 can be found in Ref.[21]. The collisional energy loss for Ar is lower than that for H_2 for electron temperatures below 10 eV. For equal input power this results in a higher electron density for Ar compared with H_2 in agreement with the observations by Gudmundsson and Kimura and Kasugai[17,20] and with our experiment with constant rf power. A more quantitative calculation of the electron density is difficult because there are unknown input parameters like, for example, the absorbed power.

F. Plasma monitor raw data

Signal intensities for different ion species detected in a pure Ar plasma and a pure H_2 plasma are shown in Fig. 9 as a function of the discriminator voltage V_{PM}. The curves are normalized to their maximum for easy comparison. They differ in the absolute energy, shape and width. While in a pure H_2 plasma the ions show a maximum at (26±1) eV the maximum is at (15±1) eV in a pure Ar plasma. The full width at half maximum (FWHM) decreases with mass starting from (6.9±0.3) eV for H^+ to (4.8±0.3) eV for H_2^+ to (3.6±0.3) eV for H_3^+ and (2.3±0.3) eV for Ar^+. The maxima as well as the FWHMs for the Ar admixed H_2 plasmas are in between the values shown in Fig. 9.

All these observations are in accordance with measurements by Gudmundsson[17]. With increasing f_{Ar} he also observed a decrease of the mean ion energy. This coincides with a decrease in the plasma potential which was directly measured in the present work using

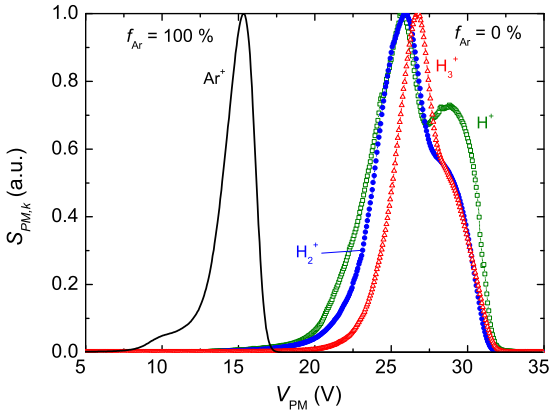

FIG. 9. Normalized ion signal intensities $S_{\mathrm{PM},k}(V_{\mathrm{PM}})$ measured with the PM for a pure Ar plasma (solid line) and a pure H_2 plasma (symbols) as a function of the discriminator voltage V_{PM} for a total pressure of 1.0 Pa.

the Langmuir probe. Furthermore, Gudmundsson also found a decrease in the FWHM with ion mass. He also found an increase of the FWHM for the same ion species with increasing f_{Ar}. He attributed this mainly to a reduced parasitic capacitive coupling due to a considerable increase in electron density with increasing Ar fraction. Here we tried to minimize such an influence by a rather small variation in electron density. We, therefore, can try to quantitatively compare the observed change in the FWHM with the theoretical expectation.

According to Gudmundsson[17] the width of the ion energy distribution is defined by the product of the ion transit time τ_{ion} and the rf period $1/\tau_{rf}$:

$$\frac{\tau_{ion}}{\tau_{rf}} = \frac{3\overline{s}}{\tau_{ion}}\sqrt{\frac{M_i}{2eV_{pl}}} = \frac{3\times 2.6}{\tau_{ion}}\sqrt{\frac{\varepsilon_0 k_B T_e M_i}{2e^3 h_l n_e V_{pl}}} \tag{36}$$

(M_i - ion mass, V_{pl} - voltage drop in the sheath, ε_0 - vacuum permittivity, k_B - Boltzmann constant, T_e - electron temperature, n_e - electron density, h_l - electron density ratio between sheath edge and plasma center). The sheath thickness is given by[67] $\overline{s_{\mathrm{H_2}}} = 2.0\ \lambda_{Ds}$ for the H_2 plasma and $\overline{s_{\mathrm{Ar}}} = 2.5\ \lambda_{Ds}$ for the H_2 plasma. The Debye length at the sheath edge is $\lambda_{Ds} = \sqrt{\varepsilon_0 k_B T_e/(e^2 n_{es})}$. Here the electron density at the sheath edge n_{es} is required which is estimated by $n_{es} = h_l n_e$ using Godyak's factor h_l (see Eqn. 10). For V_{pl} the voltage of the maxima of the curves in Fig. 9 are taken. Considering the measured T_e, n_e, M_i, and

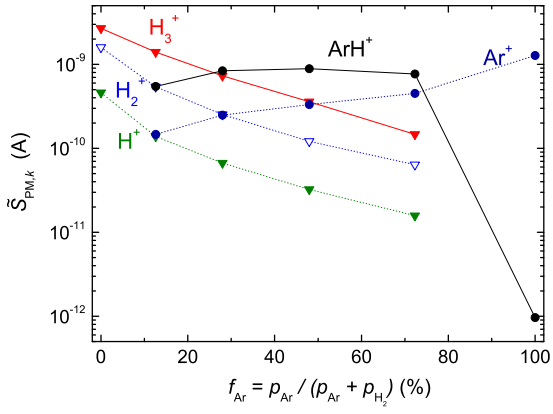

FIG. 10. Energy-integrated plasma monitor signals $\tilde{S}_{\mathrm{PM},k}$ as a function of f_{Ar} for all detected ion species. The total pressure is 1.0 Pa.

the geometry of the system we calculate for a pure H_2 plasma the ratio of the ion transit times of H_3^+ and H^+ to be 1.7 and measure a change of the FWHM of also 1.9. For H_2-Ar discharges between 12.6 and 100 % Ar we expect a constant ion transit time and would, therefore, expect to see no change of the FWHM. However, we find a continuous reduction of the FWHM with increasing f_{Ar}. Between $f_{\mathrm{Ar}} = 12.6$ % and $f_{\mathrm{Ar}} = 100$ % the FWHM decreases by 40 %. We attribute this effect to a reduced capacitive coupling which could be due to the remaining increase of the electron density with increasing f_{Ar}. The same effect was also observed by Gudmundsson[17].

In summary, for different experimental conditions (e.g. the Ar content) the ion energy distributions differ in absolute energy position and width. However, within one fix plasma condition they are comparable for all considered species. Therefore, we can apply our conversion procedure from PM raw data into absolute-quantified ion densities as outlined in Sect. III A. Before we show the mass-resolved ion densities we present the energy-integrated ion signals which is common in most publications. By comparing both, the difference between ion signals and ion densities will become evident.

G. Mass-resolved and energy-integrated ion signals

Figure 10 shows energy-integrated plasma monitor ion signals $\tilde{S}_{\mathrm{PM},k} = \int S_{\mathrm{PM},k}(V)dV$ for $k = \mathrm{Ar}^+$, H^+, H_2^+, H_3^+ and ArH^+ as a function of the Ar fraction. As expected the signal of the Ar^+ ion increases with increasing Ar content and, correspondingly, the hydrogen ion species decrease. The signals of the hydrogen ion species show all the same behavior. With increasing f_{Ar} the signals decrease nearly exponentially with the H_2 fraction. The most striking observation in Fig. 10 is the fact that even at this low pressure the dominant ion signals are from H_3^+ and ArH^+, for low and high Ar admixture respectively. The signal of the ArH^+ ion stays roughly constant over the considered composition range. This dominance is at first glance unexpected as these ions are not primary ions produced by direct electron impact such as Ar^+ and H_2^+ but secondary ions that are produced by ion-neutral collisions. The dominant production channel for H_3^+ is[33]: $\mathrm{H}_2^+ + \mathrm{H}_2 \rightarrow \mathrm{H}_3^+ + \mathrm{H}$. For ArH^+ the dominant production channel is[33]: $\mathrm{Ar}^+ + \mathrm{H}_2 \rightarrow \mathrm{ArH}^+ + \mathrm{H}$. Although the H_2 gas flow was switched off for the experiments with $f_{\mathrm{Ar}} = 100$ % we still measured a small ArH^+ signal. This is attributed to small quantities of H_2 released from the chamber walls.

The results shown in Fig. 10 can be qualitatively compared to published data. Gudmundsson[16,17] investigated an inductively coupled H_2-Ar plasma in a discharge vessel with a height of 76 mm and a diameter of 305 mm. He used a pressure of $p = 2.7$ Pa and a constant power of $P = 400$ W. No ArH^+ was reported. He measured a low (< 0.1) $\mathrm{H}^+/\mathrm{H}_2^+$ and a $\mathrm{H}_3^+/\mathrm{H}_2^+$ signal intensity ratio of about 1. In the present work similar results were obtained for the $\mathrm{H}^+/\mathrm{H}_2^+$ ion signal ratio, which is about 0.25. In the present study the $\mathrm{H}_3^+/\mathrm{H}_2^+$ ion signal ratio is higher which is confirmed by the results of[20]. Gudmundsson found that the $\mathrm{Ar}^+/\mathrm{H}_2^+$ signal intensity ratio is low ($<$ 0.1) for f_{Ar} lower than 70 % and increases to 0.6 for $f_{\mathrm{Ar}} = 90$ %. In the present study a $\mathrm{Ar}^+/\mathrm{H}_2^+$ signal intensity ratio higher than 1 for $f_{\mathrm{Ar}} > 40$ % is observed. The discrepancy can be due to good conversion of Ar^+ into ArH^+. However, it could also be due to a different mass-dependent transmission of the PM of Gudmundsson.

Jang and Lee[18] studied an inductively coupled H_2-Ar plasma at 13.56 MHz with an rf power of 800 W and pressure of 4 Pa. They used an energy-dispersive mass spectrometer to study the ion species. The Ar^+ signal was about 3 % of the ArH^+ signal and showed the same dependence on f_{Ar} as ArH^+. Both ion signals increased for increasing Ar fraction. The

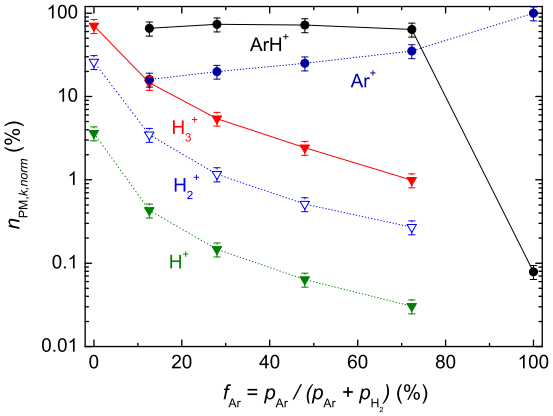

FIG. 11. Normalized ion densities $n_{\mathrm{PM},k,norm}$ as a function of f_{Ar} for a total pressure of 1.0 Pa.

H_2^+ and H^+ ions showed a nearly constant signal with varying f_{Ar}. The signal heights were between the ArH^+ and Ar^+ signals. The H_2^+ signal was slightly higher than the H^+ signal. No H_3^+ was reported. The ArH^+ signal was the dominant one for Ar fractions between 30 and 90 %. Although great care has to be taken in comparing signals from different devices and especially different energy and mass-resolved detection systems, we can state that their results are qualitatively comparable to the data shown in Fig. 10. But it has to be kept in mind that even if the ArH^+ shows the highest signal, this does not automatically mean that it is also the dominant ion species. To conclude that the mass-dependent transmission function of the plasma monitor has to be known.

Although most publications stop at such an evaluation of the plasma monitor signals and call these measurements "flux" measurements we apply in the following the procedure outlined in Sect. III A to convert these signals measured with the PM into absolutely quantified densities taken into account n_e, and T_g.

H. Ion densities

Let us first consider the mass-resolved normalized ion species composition $n_{\mathrm{PM},k,norm}$ (Eqn. 15) shown in Fig. 11 as function of the Ar fraction. Here the relative calibration procedure of the PM outlined in Sect. III A 3 was applied. In a pure H_2 plasma three ion

species occur, namely H^+, H_2^+ and H_3^+. H^+ has the lowest density with about one percent of the total ion density while H_2^+ contributes about 30 %. The dominant ion is the H_3^+ ion with a contribution of 70 %. Adding Ar, the H_x^+ densities ($x = 1, 2, 3$) decrease with increasing f_{Ar} while the ratio between then remains roughly constant. In mixed H_2-Ar plasmas the ArH^+ ion is the dominant ion and contributes about 2/3 to the total ion density in the Ar fraction range from 12.6 to 72.3 %. Ar^+ is the second most abundant ion species in this range and shows an increasing density with increasing Ar fraction. In a pure Ar plasma the argon ion density is by far dominant but there is still a very small contribution (< 0.1 %) of the ArH^+ ion. The origin of this signal is attributed to residual H_2 reacting with Ar.

Next, let us compare the integrated signal intensities $\tilde{S}_{\mathrm{PM},k}$ (Fig. 10) with the derived densities $n_{\mathrm{PM},k,norm}$ (Fig. 11): While for the pure H_2 plasma the change in ratio between H^+, H_2^+ and H_3^+ for $\tilde{S}_{\mathrm{PM},k}$ (Fig. 10) and $n_{\mathrm{PM},k,norm}$ (Fig. 11) is already substantial it becomes even more pronounced for the Ar admixed cases. The ratios between the H_x^+- and the Ar^+-related species change even more. While the H_3^+ signal in Fig. 10 is larger than or comparable to the ArH^+ signals for 12.6 and 28 % Ar fraction, respectively, Fig. 11 shows a different result. Even for the smallest investigated Ar fraction the dominant ion species is ArH^+. This change of the ratios between signal intensities and relative ion densities is due to the mass-dependent transmission of the PM as well as the conversion from fluxes into densities as outlined in sections III A 2 and III A 3, respectively. Each of these effects leads at higher masses to an increase of the densities compared with the signal intensities by about a factor of $\sqrt{M_k}$.

As final result of our experiments the mass-resolved and absolute quantified ion densities of the H_2-Ar plasma at a total pressure of 1.0 Pa are shown in Fig. 12. $n_{\mathrm{PM},abs}$ has a value of 1×10^{16} m^{-3} in a pure H_2 plasma and increases to a mean value of 2.8×10^{16} m^{-3} in the H_2-Ar mixture.

As discussed in Sect. III A 3 the absolute quantification for each composition is based on the Langmuir probe measurements and the relative contributions of the ions $n_{\mathrm{PM},k,norm}$ are those from Fig. 11. For each plasma composition we determine a calibration constant according to Eqn. 14. It turned out that in our experiments this calibration constant did not vary with Ar fraction. This indicates that the energy-dependent transmission T_{ed} was constant for this set of measurements.

Kimura and Kasugai[20] and Hjartarson et al.[21] theoretically studied inductively coupled

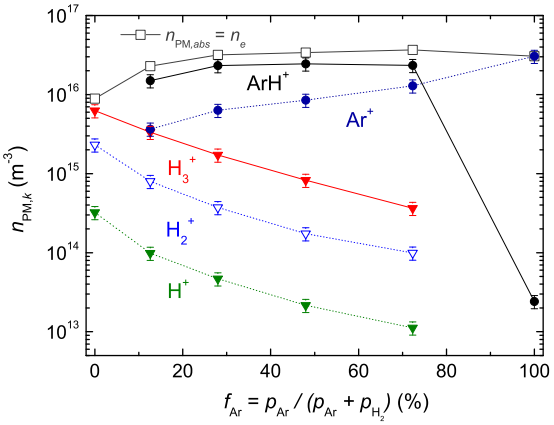

FIG. 12. Mass-resolved and absolute quantified ion densities and electron density as a function of f_{Ar} for a total pressure of 1.0 Pa.

H_2-Ar plasmas applying rate equation models to derive ion densities. In principle, both publications show rather similar trends for the variation of ion densities with changing argon fraction. Kimura and Kasugai[20] used a gas pressure of 2.7 Pa while Hjartarson et al.[21] used 1.3 Pa. Since the latter is closer to our value of 1.0 Pa we compare our measurements to the modeling results of Hjartarson et al.[21]. In contrast to our experimental observations the ArH^+ is not the dominant ion species. In their results the Ar^+ density is in the whole mixing ratio range higher than the ArH^+ density. H_3^+ is dominant for $0\ \% \leq f_{\mathrm{Ar}} < 30\ \%$ and for higher f_{Ar} the Ar^+ ion dominates. As in our experiments the H_2^+ ion is about a factor of ten lower than H_3^+. But while in our experiments H^+ is a factor of ten lower than H_2^+ it is almost equal to H_2^+ in the modeling results. The reason for these differences is presently unclear. Rate equation modeling for our specific settings are presently conducted to clarify this discrepancy.

V. CONCLUSIONS

For an energy-dispersive mass spectrometer a calibration procedure was developed to derive from mass-resolved signal intensities absolute ion densities. The calibration procedure considers the energy and mass-dependent transmission of the plasma monitor. The conversion from fluxes into densities is based on a sheath and density profile model. The

mass-dependent transmission was determined by neutral gas mass spectrometry. Only if the energy-dependent transmission is either known or constant the integrated signal is proportional to the ion flux of an individual ion species. To convert these relative fluxes to absolute fluxes an additional diagnostic such as a Langmuir probe or a retarding field analyzer is necessary.

The procedure was applied to an inductively coupled H_2-Ar plasma. In addition to the energy-dispersive mass spectrometry measurements, optical emission spectroscopy, retarding field analyzer and Langmuir probe measurments were used. The Ar fraction was varied from 0 to 100 %. The total gas pressure was 1.0 Pa. The gas temperature was derived from the rotational lines $Q_1 - Q_3$ of the Q-branch lines of the H_2 Fulcher-α diagonal band ($v' = v'' = 2$) to (540±50) K. The dissociation degree of hydrogen was determined by actinometry and was nearly constant over the considered Ar fraction range with a mean value of 1.7 ± 0.4 %. The electron temperature decreased from 5.2 eV for 0 % Ar fraction to 2.9 eV for 100 % Ar fraction. The electron density was adjusted by rf power variation around 3×10^{16} m^{-3}.

For a pure H_2 plasma the dominant ion is with about 70 % H_3^+. H_2^+ contributes about 30 % and H^+ about 1 %. For admixture with Ar the ArH^+ ion is by far the dominant ion species in a wide parameter range. Ar^+ is the second most abundant ion species in this range and shows an increasing density with increasing Ar fraction. These measurements clearly show that in low-temperature plasmas in the investigated pressure range the dominant ion species are not necessarily the primary ions which are produced by electron-induced ionization but molecular ion species which are formed by ion-molecule reactions in the gas phase.

ACKNOWLEDGMENTS

We gratefully acknowledge support from several colleagues: A. Manhard helped in the analysis of the OES data and U. von Toussaint contributed to the error determination of the plasma monitor data. The authors would like to thank T. Dürbeck and W. Hohlenburger for technical assistance.

REFERENCES

[1]A. Efremov, N. Min, J. Jeong, Y. Kim, and K. Kwon, "Etching characteristics of $Pb(Zr,Ti)O_3$, Pt, SiO_2 and Si_3N_4 in an inductively coupled HBr/Ar plasma," Plasma Sources Sci. Technol. **19**, 045020 (2010).

[2]S. Yoon, K. Tan, Rusli, and J. Ahn, "Modeling and analysis of hydrogen-methane plasma in electron cyclotron resonance chemical vapor deposition of diamond-like carbon," J. App. Phys. **91**, 40–47 (2002).

[3]I. B. Denysenko, S. Xu, J. D. Long, R. P. Rutkevych, N. A. Azarenkov, and K. Ostrikov, "Inductively coupled $Ar/CH_4/H_2$ plasmas for low-temperature deposition of ordered carbon nanostructures," J. Appl. Phys. **95**, 2713 (2004).

[4]J. Zhou, I. T. Martin, R. Ayers, E. Adams, D. Liu, and E. R. Fisher, "Investigation of inductively coupled Ar and CH_4/Ar plasmas and the effect of ion energy on DLC film properties," Plasma Sources Sci. Technol. **15**, 714–726 (2006).

[5]J. S. Kim, S. S. Jang, and W. J. Lee, Proc. Advanced Metallization and Interconnect Systems for ULSI Applications in 1995 **Materials Research Society, Pittsburgh**, 297 (1996).

[6]A. Weber, R. Nikulski, C.-P. Klages, M. Gross, R. Charatan, R. Opilan, and W. Brown, "Aspects of TiN and Ti deposition in an ECR plasma enhanced CVD process," Applied Surface Science **91**, 314 – 320 (1995), proceedings of the First European Workshop on Materials for Advanced Metallization.

[7]M. S. Ameen, J. T. Hillman, J. Faguet, R. F. Foster, C. Arena, and F. Martin, Proceedings of the Advanced Metallization for ULSI Applications in 1994 **edited by R. Blumehthel Materials Research Society, Pittsburgh**, 269 (1995).

[8]R. A. Ditizio, G. Liu, S. J. Fonash, B.-C. Hseih, and D. W. Greve, "Short time electron cyclotron resonance hydrogenation of polycrystalline silicon thin-film transistor structures," Applied Physics Letters **56**, 1140–1142 (1990).

[9]E. S. Cielaszyk, K. H. R. Kirmse, R. A. Stewart, and A. E. Wendt, "Mechanisms for polycrystalline silicon defect passivation by hydrogenation in an electron cyclotron resonance plasma," Appl. Phys. Lett. **67**, 3099 (1995).

[10]R. A. Gottscho, B. L. Preppernau, S. J. Pearton, A. B. Emerson, and K. P. Giapis, "Real-time monitoring of low temperature hydrogen plasma passivation of GaAs," J. Appl. Phys.

68, 440 (1990).

[11]J. D. Bernstein, S. Qing, C. Chan, and T.-J. King, "High dose-rate hydrogen passivation of polycrystalline silicon CMOS TFTs by plasma ion implantation," IEEE Trans. Electron Devices **43**, 1876 (1996).

[12]C.-F. Yeh, T.-J. Chen, C. Liu, J. Gudmundsson, and M. Lieberman, "Hydrogenation of polysilicon thin-film transistor in a planar inductive H_2/Ar discharge," Electron Device Letters, IEEE **20**, 223 –225 (1999).

[13]N. Fox-Lyon, G. S. Oehrlein, N. Ning, and D. B. Graves, "Hydrogenation and surface density changes in hydrocarbon films during erosion using Ar/H_2 plasmas," Journal of Applied Physics **110**, 104314 (2011).

[14]C. Hopf, A. von Keudell, and W. Jacob, "The influence of hydrogen ion bombardment on plasma-assisted hydrocarbon film growth," Diamond Relat. Mater. **12**, 85–89 (2003).

[15]V. S. Voitsenya, D. I. Naidenkova, Y. Kubota, S. Masuzaki, A. Sagara, and K. Yamazaki, "On the possibility to increase efficiency of conditioing of vacuum surfaces by using a discharge in a hydrogen-noble gas mixture," National Institute of Fusion Science **799**, 1 (2004).

[16]J. T. Gudmundsson, "Experimental studies of H_2/Ar plasma in a planar inductive discharge," Plasma Sources Sci. Technol. **7**, 330 (1998).

[17]J. T. Gudmundsson, "Ion energy distribution in H_2/Ar plasma in a planar inductive discharge," Plasma Sources Sci. Technol. **8**, 58 (1999).

[18]S. Jang and W. Lee, "Pressure and input power dependence of Ar/N_2H_2 inductively coupled plasma systems," J. Vac. Sci. Technol. A **19**, 2335 (2001).

[19]M. A. Lieberman and A. J. Lichtenberg, *Principles of plasma discharges and materials processing* (2005).

[20]T. Kimura and H. Kasugai, "Properties of inductively coupled rf Ar/H_2 plasmas: Experiment and global model," J. Appl. Phys. **107**, 083308 (2010).

[21]A. T. Hjartarson, E. G. Thorsteinsson, and J. T. Gudmundsson, "Low pressure hydrogen discharges diluted with argon explored using a global model," Plasma Sources Sci. Technol. **19**, 065008 (2010).

[22]P. A. Miller, G. A. Hebner, K. E. Greenberg, P. D. Pochan, and B. P. Aragon, "An inductively coupled plasma source for the gaseous electronics conference rf reference cell," J. Res. Natl. Inst. Stand. Technol. **100**, 427 (1995).

[23]V. A. Kadetov, *Diagnostics and modeling of an inductively coupled radio frequency discharge in hydrogen*, Phd thesis, Ruhr Universität Bochum (2004).

[24]K. Polozhiy, "Suppresion of capacitive coupling in a pulsed inductively coupled RF discharge," unpublished (2011).

[25]M. Bauer, T. Schwarz-Selinger, H. Kang, and A. v. Keudell, "Control of the plasma chemistry of a pulsed inductively coupled methane plasma," Plasma Sources Sci. Technol. **14**, 543–548 (2005).

[26]M. Bauer, T. Schwarz-Selinger, W. Jacob, and A. v. Keudell, "Growth precursor for a–C:H film deposition in pulsed inductively coupled methane plasmascontrol of the plasma chemistry of a pulsed inductively coupled methane plasma," J. Appl. Phys. **98**, 073302 (2005).

[27]W. Walcher, "Über eine Ionenequelle für massenspektroskopische Isotopentrennung," Zeitschrift für Physik **122**, 62–85 (1944).

[28]W. Poschenrieder, Private communication, 2012.

[29]P. Scheubert, U. Fantz, P. Awakowicz, and H. Paulin, "Experimental and theoretical characterization of an inductively coupled plasma source," J. Appl. Phys. **90**, 587 (2001).

[30]S. V. Dudin, A. P. Jatskov, and V. I. Farenik, Tekhnologiya i Konstruirovaniye v Elektronnoi Apparature **3**, 43 (2002).

[31]P. McNeely, S. Dudin, S. Christ-Koch, and U. Fantz, "A Langmuir probe system for high power RF-driven negative ion sources on high potential," Plasma Sources Sci. Technol. **18**, 014011 (2009).

[32]G. D. Conway, A. J. Perry, and R. W. Boswell, "Evolution of ion and electron energy distributions in pulsed helicon plasma discharges," Plasma Sources Sci. Technol. **7**, 337 (1998).

[33]A. Bogaerts and R. Gijbels, "Hybrid monte carlo—fluid modeling network for an argon/hydrogen direct current glow discharge," Spectrochimica Acta Part B **57**, 1071 (2002).

[34]J. A. S. Barata and C. A. N. Conde, "Elastic He^+ on He collision cross-section and Monte Carlo calculation of the transport coefficients of He^+ ions in gaseous helium," Nuclear Instruments ans Methods in Physics Research A **619**, 21 (2010).

[35]T. Baloniak, R. Reuter, C. Floetgen, and A. v. Keudell, "Calibration of a miniaturized retarding field analyzer for low-temperature plasmas: geometrical transparency and collisional effects," J. Phys. D **43**, 055203 (2010).

[36]D. Barton, D. J. Heason, R. D. Short, and J. W. Bradley, "The measurement and control of the ion energy distribution function at a surface in an rf plasma," Measurement Science and Technology **11**, 1726 (2000).

[37]K. Ellmer, R. Wendt, and K. Wiesemann, "Interpretation of ion distribution functions measured by a combined energy and mass analyzer," Int. J. of Mass Spectrometry **223-224**, 679 (2003).

[38]S. G. Walton, R. F. Fernsler, and D. Leonhardt, "Measurement of ion energy distributions using a combined energy and mass analyzer," Review of Scientific Instruments **78**, 083503 (2007).

[39]E. Hamers, W. van Sark, J. Bezemer, W. Goedheer, and W. van der Weg, "On the transmission function of an ion-energy and mass spectrometer," Int. J. Mass Spectrom. **173**, 91 (1998).

[40]P. Pecher, *Quantitative Bestimmung der Teilchenflüsse aus Methan-ECR-Plasmen*, Phd thesis (in German), Universität Bayreuth (1997).

[41]H. C. Straub, P. Renault, B. G. Lindsay, K. A. Smith, and R. F. Stebbings, "Absolute partial cross sections for electron-impact ionization of H_2, N_2, and O_2 from threshold to 1000 eV," Phys. Rev. A **54**, 2146 (1996).

[42]R. C. Wetzel, F. A. Baiocchi, T. R. Hayes, and R. S. Freund, "Absolute cross sections for electron-impact ionization of the rare-gas atoms by the fast-neutral-beam method," Phys. Rev. A **35**, 559–577 (1987).

[43]S. Agarwal, G. W. W. Quax, M. C. M. van de Sanden, D. Maroudas, and E. S. Aydil, "Measurement of absolute radical densities in a plasma using modulated-beam line-of-sight threshold ionization mass spectrometry," J. Vac. Sci. Technol. A **22 No. 1**, 71 (2004).

[44]H. Singh, J. W. Coburn, and D. B. Graves, "Appearance potential mass spectrometry: Discrimination of dissociative ionization products," J. Vac. Sci. Technol. A **18**, 299 (2000).

[45]V. A. Godyak, Soviet Radio Frequency Discharge Research, Delphic Associates, Falls Church, VA (1986).

[46]M. J. Druyvesteyn, Z. Phys **64**, 781 (1930).

[47]J. W. Coburn and M. Chen, "Optical emission spectroscopy of reactive plasmas: A method for correlating emission intensities to reactive particle density," J. Appl. Phys. **51**, 3134 (1980).

[48]D. Wuenderlich, S. Dietrich, and U. Fantz, "Applications of a collisional radiative model

to atomic hydrogen for diagnostic purposes," Journal of Quantitative Spectroscopy and Radiative Transfer **110**, 62 (2009).

[49]J. B. Boffard, R. O. Jung, C. C. Lin, and A. E. Wendt, "Optical emission measurements of electron energy distributions in low-pressure argon inductively coupled plasmas," Plasma Sources Sci. Technol. **19**, 065001 (2010).

[50]J. E. Chilton, J. B. Boffard, R. Scott, and C. C. Lin, "Measurement of electron-impact excitation into the $3p^5$ 4p levels of argon using Fourier-transform spectroscopy," Phys. Rev. A **57**, 267 (1998).

[51]T. Czerwiec, F. Greer, and D. B. Graves, "Nitrogen dissociation in a low pressure cylindrical ICP discharge studied by actinometry and mass spectrometry," J. Phys. D **38**, 4278 (2005).

[52]B. P. Lavrov and A. V. Pipa, "Account of the fine structure of hydrogen atom levels in the effective emission cross sections of Balmer lines excited by electron impact in gases and plasma," Optics and Spectroscopy **92**, 647 (2002).

[53]G. L. Majstorovic, N. M. Sisovic, and N. Konjevic, "Rotational and vibrational temperatures of molecular hydrogen in a hollow cathode glow discharge," Plasma Sources Sci. Technol. **16**, 750 (2007).

[54]Z. Gavare, G. Revalde, and A. Skudra, "Plasma temperature determination of hydrogen containing high-frequency electrodeless lamps by intensity distribution measurements of hydrogen molecular band," Int. Journal of Spectroscopy **2010**, 804506 (2010).

[55]U. Fantz, "Emission spectroscopy of molecular low pressure plasmas," Contrib. Plasma Phys. **44**, 508–515 (2004).

[56]V. M. Donnelly and M. V. Malyshev, "Diagnostics of inductively coupled chlorine plasmas: Measurements of the neutral gas temperature," Applied Physics Letters **77**, 2467 (2000).

[57]K. Behringer, "Diagnostics and modelling of ECRH microwave discharges," Plasma Physics and Controlled Fusion **33**, 997 (1991).

[58]G. Dieke, "Principles of plasma discharges and materials processing," Wiley Interscience (1972).

[59]K. P. Huber and G. Herzberg, "Molecular spectra and molecular structure," Van Nostrand Reinhold Company **4** (1979).

[60]J.-S. Yoon, M.-Y. Song, J.-M. Han, S. H. Hwang, W.-S. Chang, B. Lee, and Y. Itikawa, "Cross sections for electron collisions with hydrogen molecules," J. Phys. Chem. Ref. Data

37, 913 (2008).

[61]M. W. Kiehlbauch and D. B. Graves, "Modeling argon inductively coupled plasmas: The electron energy distribution function and metastable kinetics," J. Appl. Phys. **91**, 3539 (2002).

[62]E. J. Tonnis and D. B. Graves, "Neutral gas temperatures measured within a high-density, inductively coupled plasma abatement device," J. Vac. Sci. Technol. A **20**, 1787 (2002).

[63]E. Tatarova, F. M. Dias, C. M. Ferreira, and N. Puac, "Spectroscopic determination of H, He, and H_2 temperatures in a large-scale microwave plasma source," J. Appl. Phys. **101**, 063306 (2007).

[64]A. Manhard, T. Schwarz-Selinger, and W. Jacob, "Quantification of the deuterium ion fluxes from a plasma source," Plasma Sources Sci. Technol. **20**, 015010 (9pp) (2011).

[65]P. Kae-Nune, J. Perrin, J. Jolly, and J. Guillon, "Surface recombination probabilities of H on stainless steel, a-Si:H and oxidized silicon determined by threshold ionization mass spectrometry in H_2 RF discharges," Surface Science Letters **360**, L495 (1996).

[66]S. Takashima, M. Hori, T. Goto, A. Kono, and K. Yoneda, "Absolute concentration and loss kinetics of hydrogen atom in methane and hydrogen plasmas," Journal of Applied Physics **90**, 5497–5503 (2001).

[67]E. Kawamura, V. Vahedi, M. A. Lieberman, and C. K. Birdsall, "Ion energy distributions in rf sheaths; review, analysis and simulation," Plasma Sources Science and Technology **8**, R45 (1999).